

# TUMSAT-OACIS Repository - Tokyo

University of Marine Science and Technology

(東京海洋大学)

Flow visualization around small roughness elements with a hydraulic scale-up model based on Re-Fr similarity law

メタデータ	言語: eng 出版者: 公開日: 2019-04-16 キーワード (Ja): キーワード (En): 作成者: Zhu, Haijun メールアドレス: 所属:
URL	<a href="https://oacis.repo.nii.ac.jp/records/1718">https://oacis.repo.nii.ac.jp/records/1718</a>

**Master's Thesis**

**FLOW VISUALIZATION AROUND SMALL ROUGHNESS  
ELEMENTS WITH A HYDRAULIC SCALE-UP MODEL  
BASED ON RE-FR SIMILARITY LAW**

**September 2018**

**Graduate School of Marine Science and Technology  
Tokyo University of Marine Science and Technology  
Master's Course of Marine System Engineering**

**ZHU HAIJUN**



**Master's Thesis**

**FLOW VISUALIZATION AROUND SMALL ROUGHNESS  
ELEMENTS WITH A HYDRAULIC SCALE-UP MODEL  
BASED ON RE-FR SIMILARITY LAW**

**September 2018**

**Graduate School of Marine Science and Technology  
Tokyo University of Marine Science and Technology  
Master's Course of Marine System Engineering**

**ZHU HAIJUN**

## **Abstract**

The movement of the ocean is very complicated and has dramatic effects on the nearby water environment, which can influence physical, biological, or socioeconomic processes related to living marine resources. Thus, it is necessary for us to find the potential rule of the movement of the ocean. However, due to the current technological limitations, the ocean movement studies on the real scale are hard to be conducted. Hydraulic model test provides a useful method for us to simulate the real water environment, which is constructed and operated at a reduced scale and offers an alternative for examining coastal phenomena. Meanwhile, hydraulic model combines with PIV (Particle image velocimetry) method, which is a whole field, nonintrusive, indirect velocity measurement technique can obtain the velocity information with high accuracy and temporal and spatial resolution by transferring the velocity information of the flow to the velocity information of tracer particles based on algorithms.

The research area of my experiment is the boundary layer areas around the roughness surface of artificial reefs. And the motivation behind the present research is to focus on the flow visualization of simultaneous flow field information around small roughness elements by following Re-Fr similarity law. Meanwhile, we also want to find the difference of the results among Re-Fr similarity law, Reynolds similarity law and Froude similarity law.

To use Re-Fr similarity law, the relationship between kinematic viscosity and concentration should be taken into consideration. Therefore, I used CMC (Carboxymethyl cellulose) as the viscous materials to change the kinematic viscosity of solutions. and falling sphere method to find the proper relationship between kinematic viscosity and concentration of CMC solutions.

Then, I did the experiments about flow visualization around small roughness elements by following different similarity law. I totally have three groups: Reynolds similarity law group, Froude similarity law group and Re-Fr similarity law group. In each group there are three different conditions, therefore, I have totally 9 cases. In each case, I have more than 4500 frames of Re-Fr similarity cases and more than 6000 frames of Reynolds similarity law cases and Froude similarity law cases. The frame rate of each case changed from 1/100s to 1/1000s based on the velocity of the flow. Normally, the higher velocity the smaller frame rates will be used in the experiments. Then, I depicted the flow fields around the surface of roughness elements and analyzed the velocity profile of horizontal component of five different positions around the roughness elements.

The results of the whole experiments are shown as follow:

1. The relationship between the kinematic viscosity and concentration of CMC solution follows:

$$v_{cmc} = v_{water} \times (1 + 4.5 \times 10^8 \times C_{cmc}^{2.4})$$

2. The tendency of the flow fields and the thickness of boundary layer around the roughness element are similar among different similarity law but details are different.
3. Velocity gradient and boundary layer thickness are affected by the similarity laws.  
Bigger Reynolds value gives smaller velocity gradient and thicker boundary layer.  
Bigger Froude value gives bigger velocity gradient and thinner boundary layer.
4. Vortex flow:

In crest areas, vortex flow only appears in Re-Fr and Fr similarity law cases.

In the trough areas, the return flow appears in all cases

# Contents

<b>Abstract .....</b>	<b>I</b>
<b>Chapter 1: Introduction .....</b>	<b>1</b>
1.1 General introduction.....	1
1.2 Flow visualization .....	4
1.3 Hydraulic model.....	4
1.3.1 Theory of models .....	5
1.3.2 Model scales.....	6
1.3.3 Distorted models .....	6
<b>Chapter 2: Hydraulic scale-up similarity law .....</b>	<b>8</b>
2.1 Similarity law .....	8
2.2 Literature Review .....	13
2.3 Motivation and objective.....	13
<b>Chapter 3: Method to control kinematic viscosity .....</b>	<b>14</b>
3.1 Background .....	14
3.2 Experiments:.....	17
3.2.1 Experimental set-up and procedure.....	17
3.2.2 Data processing .....	22
3.3 Results .....	23
3.3 Discussion and conclusion .....	25
<b>Chapter 4: Application of Re-Fr scale-up model.....</b>	<b>27</b>

4.1 Introduction .....	27
4.2 Experiments.....	28
4.2.1 Experimental purpose .....	28
4.2.2 Experimental set-up and instrument .....	28
4.2.3 Experimental conditions and procedure.....	34
4.3.4 Data processing .....	36
4.3 Results .....	38
4.4 Discussion and conclusion .....	53
<b>Chapter 5: Conclusions and limitations .....</b>	<b>54</b>
<b>Acknowledgment .....</b>	<b>55</b>
<b>References.....</b>	<b>57</b>
<b>Appendix .....</b>	<b>61</b>
Appendix A: PIV method .....	61
Principle of Particle Image Velocimetry (PIV) .....	61
Image evaluation method for PIV .....	63
Appendix B: program.....	67
Case 1500_2.a.m.....	67
Outputimage.m.....	70

# **Chapter 1: Introduction**

## **1.1 General introduction**

Artificial reef is widely used to improve marine ecological environment. Some fisheries developed countries, such as America, Japan, Korea, Australia, New Zealand and EU states have acquired a lot of achievements on the exploitation and protection of fishery resources of artificial reefs. Flow field effect, bait effect and avoidance effect will be caused when the artificial reefs are placed on the sea floor (Tang et al,2017). One of the main functions of artificial reefs are to enhance the biodiversity of nearby water areas by attracting mature fish around them or small wildlife such as larvae or spores of seaweeds attach to the roughness surface.

A comprehensive literature review is undertaken of global artificial reefs, their design, application and management by professor Mark Baine in 2001. The European Artificial Reef Research Network (EARRN) defines an artificial reef as a submerged structure placed on the substratum (seabed) deliberately, to mimic some characteristics of a natural reef (Jensen,1998). Their use as a tool in coastal management has many general purposes including deployment in Japan to increase fisheries yield and production (Tsumura et al, 1999), recreational diving in the United States (Ditton et al,1999), and the prevention of trawling in Europe (Relini, 2000). Artificial reef reviews do exist (Seaman,1996) although varying in their focus and objectivity.

In fluid mechanics, boundary layer is a very important concept, which was presented in a classic paper by Prandtl (1904). He introduced the concept of a “fluid boundary layer,” which laid the foundation for the unification of the theoretical and experimental aspects of fluid mechanics.

Boundary layer is a thin layer of moving fluid near a solid surface in which the no-slip condition and viscosity combine to create a velocity gradient, which is regarded as one of the most dynamic regions (Shaughnessy, 2005). As illustrated in Figure 1.1. The fluid at the plate surface does not move relative to the plate. A short distance away from the plate, however, the fluid is moving at the free stream velocity. The effect of viscosity is to create a boundary layer near the flat plate in which the velocity changes smoothly and continuously from zero on the flat plate to the free stream value (Shaughnessy, 2005). The characteristics of a boundary layer are affected by the shape of the solid surface of interest. The orientation of the surface relative to the freestream, and many factors. Observation shows that at large Reynolds numbers the boundary layer is thin, and the thickness of the boundary layer increases in the downstream direction. Moreover, just downstream of the nose of the plate the boundary layer is observed to be laminar, but at some point downstream transition occurs and the boundary layer becomes turbulent. (Shaughnessy, 2005)

The importance of the boundary layer area is widely recognized, one main reason is the movement of small wildlife take place in it, and more importantly, this water environment will also influence the final attachment of small creature on the surface, which can influence physical, biological, or socioeconomic processes related to living marine resources in the certain areas. However, the characteristics of the boundary layers are affected by the shape of the roughness surface of the interest. Therefore, how does the roughness elements of the surface influence the boundary layer and the potential movement in the boundary layer areas is of vital importance.

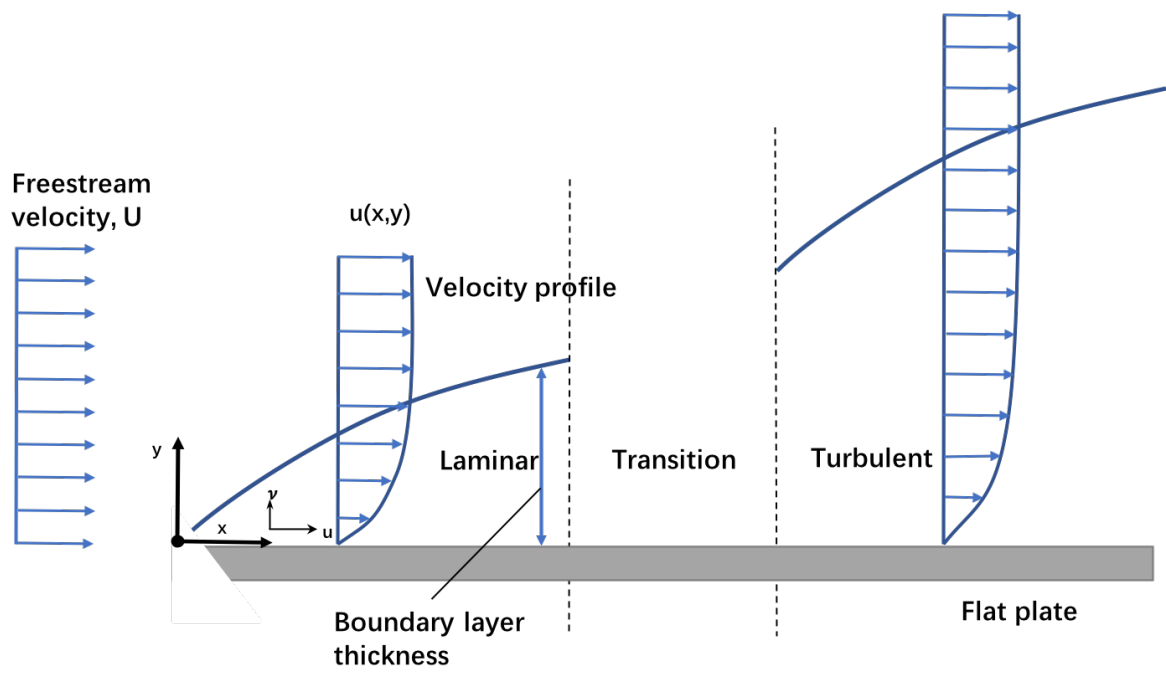


Figure 1.1 Geometry for flow over a flat plate (From Shaughnessy, 2005)

## **1.2 Flow visualization**

Flow visualization in fluid dynamics is used to make the flow pattern visible, to get information on them. It is one of the most effective tools in flow analysis, and it has been crucial to improve the understanding of complex fluid flows. The main method to make flow visualization includes: surface flow visualization method, particle tracer method and optical methods (From Wikipedia), which is an indirect method since the researchers observe the motion of the other materials (such as tracer particles) instead the fluid itself. Therefore, the difference between the fluid movement and that other outer materials is inevitable.

The application of flow visualization and its technique are widely used in engineering sciences and experimental physics. Most fluids, gaseous or liquid, are transparent media, and their motion remains invisible to the human eyes during a direct observation. In order to be able to recognize the motion of the fluid, one must provide a certain technique by which the flow is made visible. Such methods are called flow visualization techniques (Merzkirch, 2012).

## **1.3 Hydraulic model**

A physical model is a physical system reproduced (usually at a reduced size) so that the major dominant forces acting on the system are represented in the model in correct proportion to the actual physical system (Hughes,1993). Models are widely used in fluid mechanics and a model is a representation of a physical system that may be used to predict the behavior of the system in some desired respect. The physical system for which the predictions are to be made is called the prototype. In general, models resemble the prototype but have different size and variable conditions such as viscosity, velocity and so on. Normally, researchers use the scale-down model, which means the test models are smaller

than the prototype. Therefore, it is more convenient and less expensive to operate in a relatively smaller size such as in the laboratory than a large prototype. Occasionally, if the size of prototype is very small, we also use the scale-up model, which means the test models are larger than the prototype to help us observe and analyze the related phenomenon.

### 1.3.1 Theory of models

The theory of models will be described in the following chapter by following the ideas of Munson B R, et al, which presented in the book named *Fundamentals of Fluid Mechanics*.

The theory of models can be readily developed by using the principles of dimensional analysis (Abbreviated as DA), which is a foundation of the theories of similitude and modeling, and it provides a method to design an efficient experimental program. The basic principle of DA is that all terms of physical equation must have the same dimensions. It has been shown (Eq.1.1) that any given problems can be described in terms of a set of Pi terms as:

$$\pi_{1p} = \Phi(\pi_{2p}, \pi_{3p}, \pi_{4p}, \dots, \pi_{np}) \quad (1.1)$$

One of advantages of Pi theorem is that we don't need the specific variable values. If Eq.1.1 describes a situation of a certain prototype, correspondingly, the relationship of model can be written as Eq.1.2:

$$\pi_{1m} = \Phi(\pi_{2m}, \pi_{3m}, \pi_{4m}, \dots, \pi_{nm}) \quad (1.2)$$

where the form of the function will be the same if the same phenomenon is involved in both the prototype and the model. Variables, or pi terms, without a subscript will refer to the prototype, the form of  $\Phi$  is same between the prototype and model, therefore, Eq.1.3 is the

desired prediction equation and Eq.1.4-Eq.1.7 named as the model design conditions, also called similarity requirements or modeling laws.

$$\pi_{1p} = \pi_{1m} \quad (1.3)$$

$$\pi_{2p} = \pi_{2m} \quad (1.4)$$

$$\pi_{3p} = \pi_{3m} \quad (1.5)$$

$$\pi_{4p} = \pi_{4m} \quad (1.6)$$

⋮

$$\pi_{np} = \pi_{nm} \quad (1.7)$$

### 1.3.2 Model scales

I define the ratio of the length variables between the test model and prototype as the length scale ( $L_m/L_p$ ). Other scales such as velocity scale ( $V_m/V_p$ ), viscosity scale ( $\nu_m/\nu_p$ ), density scale ( $\rho_m/\rho_p$ ) and so on. In this study, I will designate the length scale as,  $\lambda_L$  and other scales as  $\lambda_\rho$ ,  $\lambda_\nu$ , and so on, where the subscript indicates the scale. For example, if  $\lambda_L = L_m/L_p = 10$ , which means the test model is 10 times bigger than the prototype.

Where  $L$  is the geometric scale,  $V$  is the velocity,  $\nu$  is the kinematic viscosity,  $\rho$  is the density and  $\lambda$  is the length scale between test model and prototype.

### 1.3.3 Distorted models

When we use the hydraulic model to simulate the prototype of the reality, it is very difficult to satisfy all the requirements. If one or more of the similarity requirements are not met, for example, if  $\pi_{2p} \neq \pi_{2m}$ , then it follows that the prediction equation  $\pi_{1p} = \pi_{1m}$  is not true; that is,

$\pi_{1p} \neq \pi_{1m}$ . Models for which one or more of the similarity requirements are not satisfied are called distorted models (Fundamentals of Fluid Mechanics (Munson B R,2012)).

## **Chapter 2: Hydraulic scale-up similarity law**

Hydraulic model test provides a conducive method for us to simulate the real water environment, which constructed and operated at reduced scale and offer an alternative for examining coastal phenomena that are presently beyond our analytical skills (Hughes 1993).

### **2.1 Similarity law**

The hydraulic similarity law is presented to provide an effective method to make the results of hydraulic model test reliable between test model and prototype. If we would like to use test model to simulate the prototype, the similarity law, such as geometric similarity, kinematic similarity and dynamic similarity, must be met and only all these conditions are satisfied, we consider the test model and prototype are completely similar, then it is possible to use the test model to simulate the whole-scale device and to get reliable results.

By nondimensionalizing the governing equations, the solution to a flow problem in a specified geometry depends only on the values of the relevant nondimensional groups that appears in the transformed equations and boundary conditions, which means that given solution to the governing equations applies to any geometrically similar flow that has the same value for the dimensionless groups. Thus, the solution applies to a flow with a different length scale but whose other scales are adjusted in such a way that the dimensionless groups are same. More importantly, the nondimensional governing equations for two physical systems that are geometrically similar are identical if the values of the dimensionless groups are identical. This proves that the flows are dynamically similar when the values of each dimensionless groups are same (Shaughnessy, 2005).

The common variables and dimensionless groups in fluid mechanics such as Mach number, Euler number show in Table 2.1. Different dimensionless groups should be chosen based on various situations. Considering the experimental condition, Reynolds number, Froude number are possible to be applied in my experiments, where Froude number is applied in open channel flow and Reynolds number is applied in flow around small objects. My experiments are open channel and used to simulate small scale objects. Meanwhile, the viscosity force, inertia force and gravitational force are the top three important factors. Therefore, I choose Reynolds number and Froude number to consist of Re-Fr similarity law to do the hydraulic scale up model test.

Table 2.1 Common dimensionless groups in fluid mechanics (Munson,2006)

Dimensionless Groups	Name	Physical meaning	Applications
$\frac{\rho VL}{\mu}$	Reynolds number, Re	$\frac{\text{inertia force}}{\text{viscous force}}$	Generally of importance in all types of fluid dynamics problems
$\frac{V}{\sqrt{gL}}$	Froude number, Fr	$\frac{\text{inertia force}}{\text{gravitational force}}$	Flow with a free surface
$\frac{P}{\rho V^2}$	Euler number, Eu	$\frac{\text{pressure force}}{\text{inertia force}}$	Problems in which pressure, or pressure differences, are of interest
$\frac{\rho V^2}{E_v}$	Cauchy number, Ca	$\frac{\text{inertia force}}{\text{compressibility force}}$	Flows in which the compressibility of the fluid is important
$\frac{V}{c}$	Mach number, Ma	$\frac{\text{inertia force}}{\text{compressibility force}}$	Flows in which the compressibility of the fluid is important
$\frac{\omega L}{V}$	Strouhal number, St	$\frac{\text{inertia(local) force}}{\text{inertia(convective) force}}$	Unsteady flow with a characteristic frequency of oscillation
$\frac{\rho V^2 L}{\sigma}$	Webber number, We	$\frac{\text{inertia force}}{\text{surface tension force}}$	Problems in which surface tension is important

According to Reynold similarity law, if we only change the length scale ( $\lambda_L = L_m/L_p$ ) of the velocity( $U$ ) and water depth( $h$ ) but neglect the influence of viscosity ( $\nu_p = \nu_m$ ;  $U_p = U_m \lambda_L$ ;  $h_p = h_m/\lambda_L$ ). The derivation processes are shown from Eq.2.1 to Eq.2.6, which means only the Reynolds number can have a same value between the prototype and model, but Froude number cannot have the same value. On the contrary, if change the related parameters by following Froude similarity law, the result shows in Eq.2.7-Eq.2.12, which can only make the Froude number have a same value between the prototype and test model, but Reynolds number cannot. That means if we follow Re similarity law or Fr similarity law respectively, then we cannot get a completely simulated value between the prototype and test model. However, to simulate the real natural environment completely and properly, we are supposed to satisfy Reynolds similarity law and Froude similarity law, simultaneously. Thus, we developed Re-Fr similarity law, change the length scale( $\lambda_L$ ) among viscosity( $\nu$ ), velocity ( $U$ ) and water depth( $h$ ), the derivation progresses are shown from Eq.2.13 to Eq.2.18. From the results, we find that the results can not only satisfy Reynolds similarity law but also satisfy Re-Fr similarity law. Thus, theoretically speaking, if we simulate the prototype by following Re-Fr similarity law, then it will present a better result than follow Reynolds similarity law and Froude similarity law.

$$\lambda_L = \frac{L_m}{L_p} \quad (2.1)$$

$$\nu_p = \nu_m \quad (2.2)$$

$$U_p = U_m \lambda_L \quad (2.3)$$

$$h_p = \frac{h_m}{\lambda_L} \quad (2.4)$$

$$Re_p = \frac{U_p h_p}{\nu_p} = \frac{U_m \lambda_L \times \frac{h_m}{\lambda_L}}{\nu_m} = Re_m \quad (2.5)$$

$$Fr_p = \frac{U_p}{\sqrt{gh_p}} = \frac{U_m \lambda_L}{\sqrt{\frac{h_m}{\lambda_L}}} = \lambda_L^{\frac{3}{2}} Fr_m \quad (2.6)$$

Where subscript p means the prototype, m means the model.

$$\lambda_L = \frac{L_m}{L_p} \quad (2.7)$$

$$v_p = v_m \quad (2.8)$$

$$U_p = \frac{U_m}{\sqrt{\lambda_L}} \quad (2.9)$$

$$h_p = \frac{h_m}{\lambda_L} \quad (2.10)$$

$$Re_p = \frac{U_p h_p}{v_p} = \frac{\frac{U_m}{\sqrt{\lambda_L}} \times \frac{h_m}{\lambda_L}}{v_m} = \lambda_L^{\frac{3}{2}} Re_m \quad (2.11)$$

$$Fr_p = \frac{U_p}{\sqrt{gh_p}} = \frac{\frac{U_m}{\sqrt{\lambda_L}}}{\sqrt{g \frac{h_m}{\lambda_L}}} = Fr_m \quad (2.12)$$

Where subscript p means the prototype, m means the model.

$$\lambda_L = \frac{L_m}{L_p} \quad (2.13)$$

$$v_p = \frac{1}{\lambda_L^{\frac{3}{2}}} v_m \quad (2.14)$$

$$U_p = \frac{1}{\sqrt{\lambda_L}} U_m \quad (2.15)$$

$$h_p = h_m \frac{1}{\lambda_L} \quad (2.16)$$

$$Re_p = \frac{U_p h_p}{v_p} = \frac{\frac{1}{\sqrt{\lambda_L}} U_m \times h_m \frac{1}{\lambda_L}}{\frac{1}{\lambda_L^{\frac{3}{2}}} v_m} = Re_m \quad (2.17)$$

$$Fr_p = \frac{\frac{1}{\sqrt{\lambda_L}} U_m}{\sqrt{g h_m \frac{1}{\lambda_L}}} = Fr_m \quad (2.18)$$

Where subscript p means the prototype, m means the model.

Theoretically speaking, Re-Fr similarity law is more reliable than Reynolds similarity law and Froude similarity law, which can satisfy Reynolds number and Froude number simultaneously. However, the problem to use Re-Fr similarity law is how to change the kinematic viscosity to satisfy the relationship (Eq.2.14) between scale length and scale of kinematic viscosity.

## 2.2 Literature Review

Other experiments on flow visualization around small roughness elements of artificial reefs were made in 2017. The research purpose is to find the flow fields of the boundary layer areas on the surface of artificial reefs. In his experiments, he used hydraulic scale-up model test based on Reynolds similarity law. Considering Reynolds similarity law obviously mentions viscous effect. What he didn't follow was Froude similarity law, which means he didn't consider gravity effects

*Numerical simulation of effect of guide plate on flow field of artificial reef (2016)* were made to find the new design idea for artificial reefs. *Effects on algal density of substrate roughness and sediment (2016)* were made to the effect of sediment and roughness and the interaction between them on algal density depends on the algal species and substrate materials. *The effect of substrate roughness and sediment on algal spore attaching ability and sporeling density (2014)* were made to find the effects of substrate roughness on spore attachment and seedling densities.

The methods of these experiments mentioned above, are only take Reynolds number into consideration. However, as for the experiment I think the Froude number is an inevitable factor which has a great effect on the reliability of the simulating results.

## 2.3 Motivation and objective

The objectives of this paper are involved in two aspects. One is to use Re-Fr similarity law in my experiment by changing the kinematic viscosity of liquid to satisfy the relationship between scale of kinematic viscosity and geometric scale, another is to simulate the flow fields around the roughness surface of artificial reefs by using PIV methods.

## Chapter 3: Method to control kinematic viscosity

### 3.1 Background

Hydraulic test model provides us an effective method to simulate the reality of the nature. If we would like to use hydraulic scale-up model by following Re-Fr similarity law to simulate the prototype completely, we must make Reynolds number and Froude number have the same value between test model and prototype. However, in constant viscosity and constant density flow, we can't only change the velocity and length scale to satisfy it. Therefore, we should change some parameters to make both Reynolds number and Froude number have the same value between the test model and prototype, respectively. Considering our experimental condition, I finally chose to change the viscosity to achieve the above results. And the derivation of relationship between viscosity and geometric scale as follows:

According to Froude similarity law:

$$\frac{U_m}{\sqrt{g_m h_m}} = \frac{U_p}{\sqrt{g_p h_p}} \quad (3.1)$$

If the model and prototype are operated in the same gravitational field, then the required velocity scale is

$$\frac{U_m}{U_p} = \sqrt{\frac{h_m}{h_p}} = \sqrt{\lambda_L} \quad (3.2)$$

According to Reynolds similarity law:

$$\frac{\rho_m U_m L_m}{\mu_m} = \frac{\rho_p U_p L_p}{\mu_p} \quad (3.3)$$

The velocity scale is

$$\frac{U_m}{U_p} = \frac{\mu_m \rho_p L_p}{\mu_p U_m L_m} \quad (3.4)$$

Since the velocity scale must be equal to the square root of the length scale, the results are as follow:

$$\frac{\mu_m / \rho_m}{\mu_p / \rho_p} = \frac{v_m}{v_p} = (\lambda_L)^{\frac{3}{2}} \quad (3.5)$$

Generally, hydraulic models of this type are distorted and are designed based on the Froude number and Reynolds number named hydraulic model based on Re-Fr similarity law. Therefore, to apply this similarity law, we are supposed to find a material to change the viscosity of the liquid by following the relationship between the scale of dynamic viscosity and scale of length.

Carboxymethyl cellulose (CMC) is a cellulose derivative with carboxymethyl groups (-CH<sub>2</sub>-COOH) bound to some of the hydroxyl groups of the glucopyranose monomers that make up the cellulose backbone, which is widely used in food and non-food products such as ice cream, diet pills and industry. As a viscous materials CMC can be dissolved in the water, non-toxic, colorless and tasteless. More importantly, the viscosity of CMC can be changed with the concentration of CMC solution, therefore, we can use it mix aimed viscosity liquid. Figure 3.1 and Figure 3.2 shows CMC materials and CMC solutions (concentration=1%).

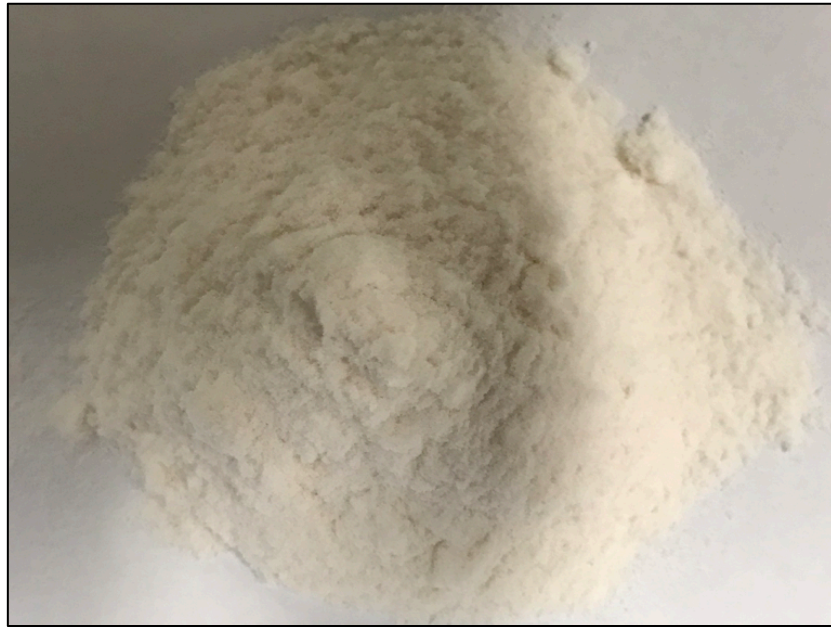


Figure 3.1 CMC materials



Figure 3.2 CMC solutions (0.1%)

## **3.2 Experiments:**

The experiments were aimed to find the relationship between the kinematic viscosity and concentration of CMC solutions which carried out in Tokyo University of Marine Science and Technology.

### **3.2.1 Experimental set-up and procedure**

The experimental set-up shows in the photo of Figure 3.3. The container, see Figure.3.3, is a colorless transparent plastic box whose size is 5cm×5.2cm×30.5cm (inner distance) and the thickness of the materials is 0.4cm. In the front size of the container, there are four lines to help me make calibration and the distance between each two lines is 2.5cm. In the top side of the box, see Figure 3.5, there is a tape (6cm×2.25cm) to help me find the drop position and make sure every time drop sphere in the same position.

The Type of CCD camera is HAS-D72 made by DITECT, which bought in 2016. The name of the software is HAS-XViewer (version1.1.0). Combined CCD camera with HAS-XViewer, we can change the windows size, frame rate and shutter speed of the frames (Details about the device shows in Table 4.1) . After getting the frames of the falling spheres, I input all frames to the software named motion studio to get the time history of the spheres while falling from the top to the bottom of the container. Figure 3.6 shows the progress of falling sphere in container (black dots is the pixel of the image).

Table 3.1 shows the parameters of the spheres and Figure. 3.7-Figure 3.8 shows the picture of the spheres. All the spheres divided into two groups one is glass spheres the other is acrylic spheres. In each group, there are three different spheres based in their size.



Figure 3.3 The photo of the experimental set-up

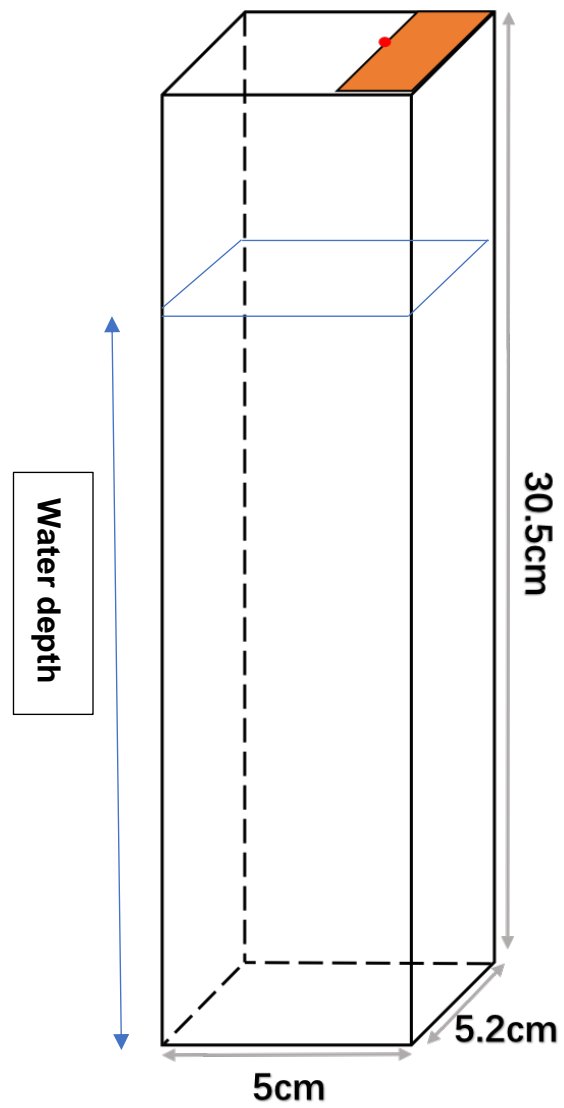


Figure 3.4 The sketch of the container

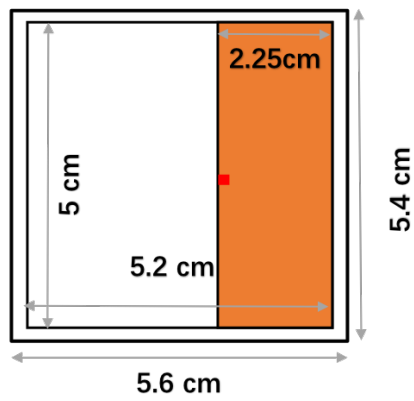


Figure 3.5 The sketch of the container of the top face



Figure 3.6 The movement of the falling sphere in the container

Table 3.1 Parameters of the falling spheres

Type	Diameter(cm)	Density(g/cm <sup>3</sup> )
Glass 1	1.62	
Glass 2	1.03	2.81
Glass 3	0.64	
Acrylic 1	0.93	
Acrylic 2	0.44	1.28
Acrylic 3	0.31	



Figure 3.7 The photo of the Acrylic spheres



Figure 3.8 The photo of the Glass spheres

The whole progress of falling sphere experiment divided into two parts.

Firstly, mix 2L CMC solution, whose concentration is from 0.1% to 0.5%. After mixed well, pour the CMC solution into the container. To avoid the influence of initial speed. The solution depth should high enough (28.5cm) and every time the sphere should be stable at the same point (middle of the tape) and move slowly to the solution to shrink the influence of initial velocity.

Then, I chose six different spheres as the falling spheres to drop them into container one by one in different CMC concentration solutions, and use the high-speed CCD (charge coupled device) camera to capture the track of the movement of the spheres and save them in the file as frames.

Finally, I used the software named motion studio to capture the related parameters such as time and position of the sphere to write in the dataset.

### 3.2.2 Data processing

According to the traditional falling sphere method, firstly we used Eq.3.6 to calculate the value of drag coefficient ( $C_D$ ), as Eq. 3.6 shows, except the value of  $C_D$ , the other variables can be easily obtained by the above experiment. Thus, I firstly calculate the value of drag coefficient,  $C_D$ .

$$(s + C_m) \frac{du}{dt} = (s - 1)g - C_D \frac{A u^2}{V} \quad (3.6)$$

Where,  $s$  is the specific gravity (the ration of density between sphere and liquid),  $C_m$  is the added mass coefficient, in my case  $C_m = 0.5$ ,  $\frac{du}{dt}$  is the acceleration of the sphere,  $g$  is the gravity force,  $A$  is the area of sphere is the volume of the sphere and  $u$  is the falling velocity of spheres.

Then according to Stokes equation,  $C_D = 24/Re$ , we can finally obtain the value of Re and Reynolds number is a function of kinematic viscosity ( $Re=UL/\nu$ ). Therefore, we can easily calculate the value of kinematic viscosity ( $Re<1$ ).

However, in my experiments, the Reynolds value is bigger than one. Therefore, the traditional way to calculate kinematic value by using falling sphere method cannot be used. Thus, after calculating the value of drag coefficient, I used Eq. 3.7 (Morrison, 2017) to calculate the value of Reynolds number then, depicted the Figure 3.10 to get the relationship between  $C_D$  and Re ( $1<Re<10^6$ ).

$$C_D = \frac{24}{Re} + \frac{2.6 \frac{Re}{5.0}}{1 + \frac{Re}{5.0}} + \frac{\left(0.411 \frac{Re}{2.63 \times 10^5}\right)^{-7.84}}{1 + \left(\frac{Re}{2.63 \times 10^5}\right)^{-8.00}} + \frac{0.25 \left(\frac{Re}{10^6}\right)}{1 + \left(\frac{Re}{10^6}\right)} \quad (3.7)$$

Where  $1<Re<10^6$

### 3.3 Results

Reynolds number is a ratio between inertial force and viscosity force whose equation has been shown in the above chapter. Therefore, after obtained the value of Reynolds number, it is easily for us to calculate the proper value of kinematic viscosity. The results between drag coefficient and Reynolds number followed by Figure 3.10 and the relationship between concentration and viscosity of CMC solutions of my experiments shows in Table 3.2. Meanwhile, Figure 3.11 shows the relationship between concentration and kinematic viscosity of CMC solutions in Log-Log coordinate system

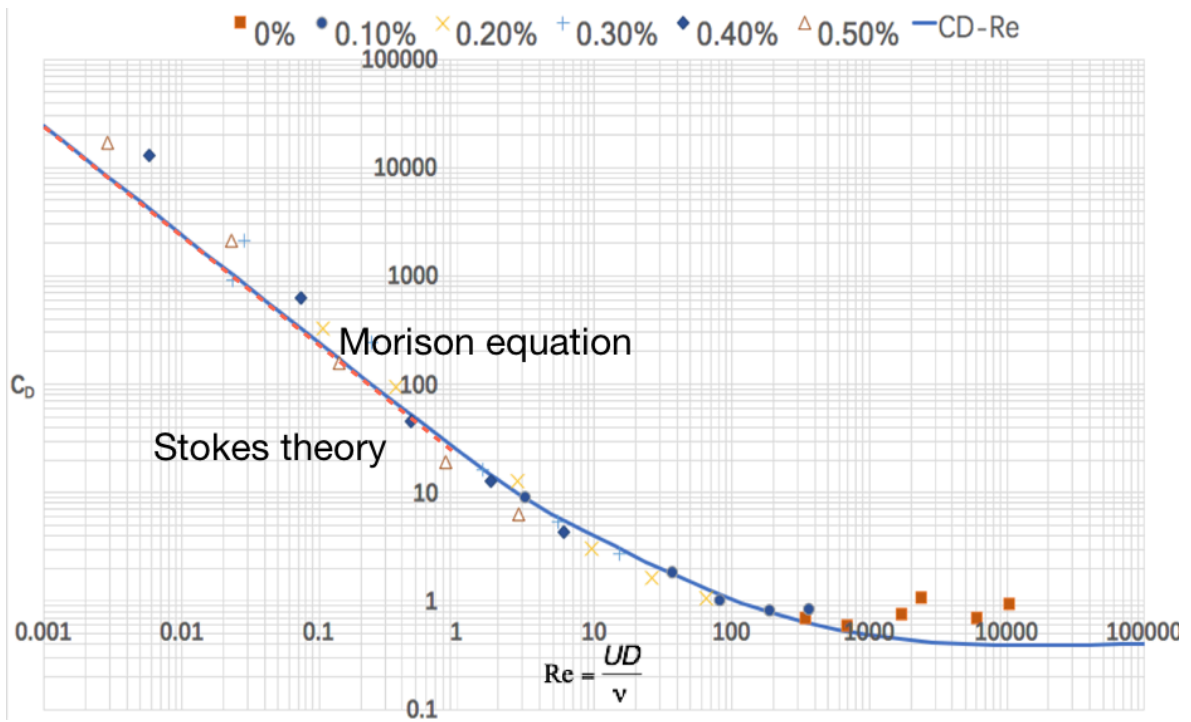


Figure 3.10 The relationships between  $C_D$  and  $Re$  in five different CMC solutions

Table 3.2 The relationships between concentration and kinematic viscosity

concentration(g/cm <sup>3</sup> )	viscosity(cm <sup>2</sup> /s)
0.10%	0.3
0.20%	1.5
0.30%	4
0.40%	8
0.50%	14

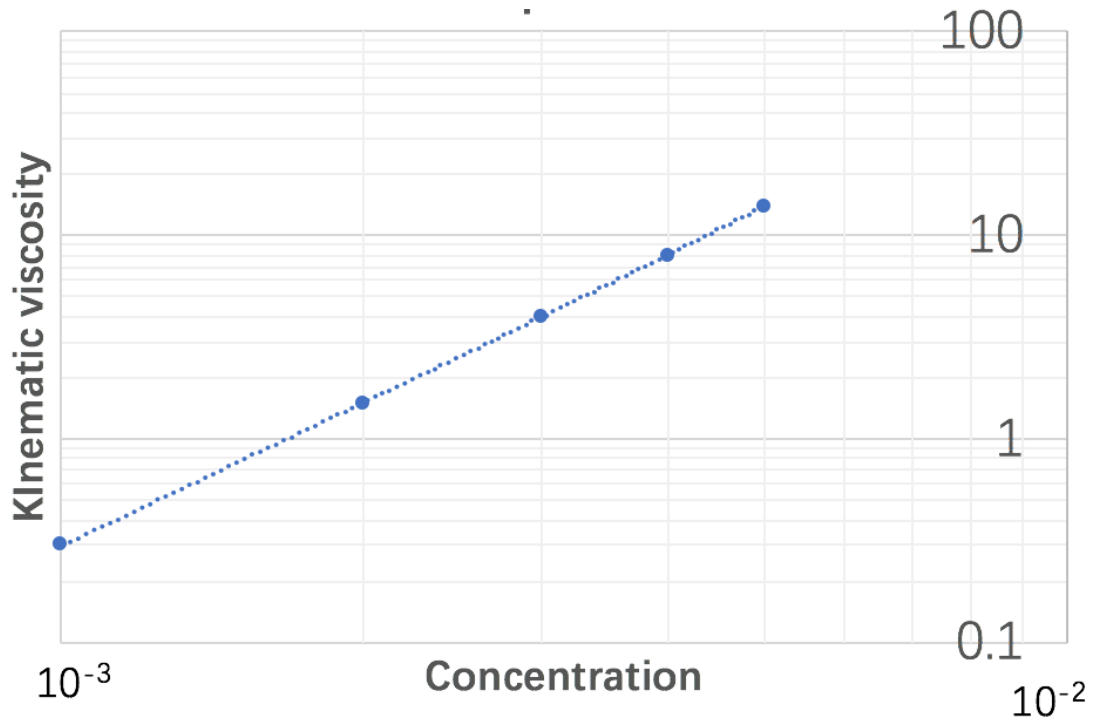


Figure 3.11 The relationship between concentration and viscosity(cm<sup>2</sup>/s) of CMC solutions in Log-Log coordinate system

### 3.3 Discussion and conclusion

As I mentioned above, to use the hydraulic scale-up model by following Re-Fr similarity law, it is necessary for us to satisfy the relationship between kinematic viscosity and concentration (Eq3.5.). After doing the above experiments, the relationship between viscosity of CMC solution and concentration of CMC solution follows Eq.3.3. The value of kinematic viscosity of water is 0.01cm<sup>2</sup>/s, therefore, if we mix a certain concentration CMC solution (0.1%<C<0.5%) then, we can easily calculate the value of viscosity followed by Eq.3.3. Meanwhile, some presentative value of the relationship among length scale, kinematic viscosity and concentration of CMC solutions are shown as Table 3.3.

$$\frac{(v_{cmc} - v_{water})}{v_{water}} = 4.5 \times 10^8 C_{cmc}^{2.4} \quad (0 < C < 0.005) \quad (3.3)$$

Where  $\nu_{cmc}$  means the kinematic viscosity value of CMC solution and  $\nu_{water}$  means kinematic viscosity value of water and  $C_{cmc}$  means the concentration value of CMC solution.

Table 3.3 Relationship between concentration and kinematic viscosity of CMC solutions

$L_r$	$\nu$ ( $\text{cm}^2/\text{s}$ )	$C_{cmc}$
1	0.01	0%
5	0.1	0.06%
10	0.3	0.10%
30	1.5	0.20%
50	4	0.30%
80	8	0.40%
120	14	0.50%

## **Chapter 4: Application of Re-Fr scale-up model**

### **4.1 Introduction**

As the above chapter discussed, if we want to simulate the prototype (natural environment) by using hydraulic model, it is necessary for us to obey similarity law. If we change the geometric scale and velocity by following Reynolds similarity law or Froude similarity law, respectively, we found that it can't simulate the prototype completely, therefore, we combined Reynolds number and Froude number to consist a new similarity law named Re-Fr similarity law. According to Re-Fr similarity law we not only need to change the scale of velocity and length scale but also need to change the scale of kinematic viscosity Therefore, I did the experiment in chapter three and found the proper value of kinematic viscosity in different CMC solution (0.1%~0.5%).

The application experiment described in this chapter was carried out in coastal environmental and engineering laboratory of Tokyo University of Marine Science and Technology. The purpose of the application experiment is to verify the reliability of Re-Fr similarity law by using PIV method to compare with the results of Re similarity law and Froude similarity law.

## **4.2 Experiments**

The experiment was carried out in Coastal Environment and Engineering Laboratory of Tokyo University of Marine Science and Technology. The details information of my experiments such as the purpose, set-up, data analyzing, and results will be described in the following part.

### **4.2.1 Experimental purpose**

The experiment of Re-Fr similarity law to small roughness elements by using PIV method is an application of hydraulic scale-up model based on Re-Fr similarity law, which has been discussed in the above chapter. I did this experiment to verify the reliability of hydraulic scale-up model based on Re-Fr similarity law make a comparison among Reynolds similarity law case and Froude similarity law case by depicting the velocity fields and velocity profile.

### **4.2.2 Experimental set-up and instrument**

Figure 4.1 shows the sketch of experimental setup, which involves three parts: High-speed CCD camera system, laser system and flume system. The size of the flume is 480cm\*30cm\*15cm (inner length of the flume). The flume is fronted by a gate which can move to adjust the water depth in the water. I used a glass pad as the gate whose size is 50 cm\*15 cm\*0.5 cm and its photo shows in Figure 4.2. Meanwhile, the information of the laser system shows in Figure 4.4.

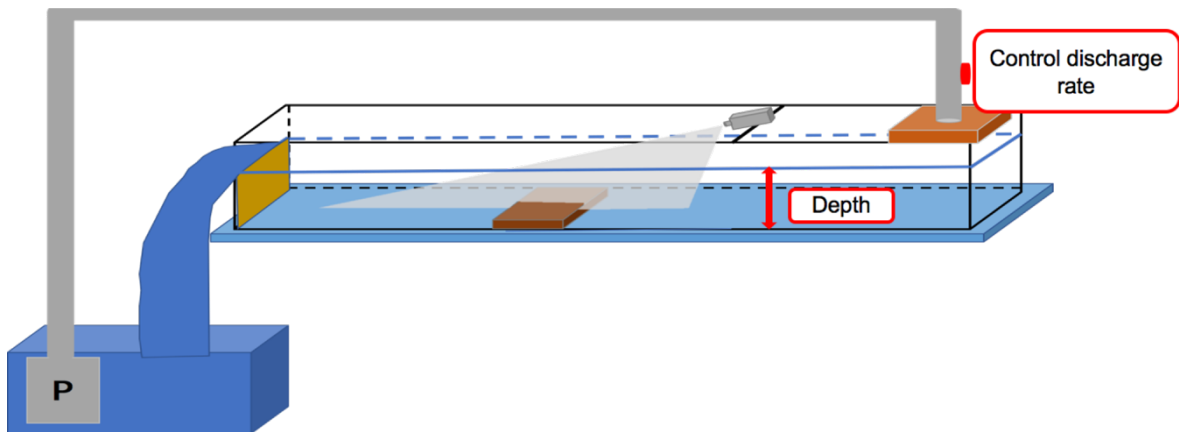


Figure 4.1 Sketch figure of the experimental set-up

The Type of high-speed CCD camera HAS-D72 made by DITECT was used. Its maximum frame rate is 2000 fps with the maximum resolution 1024×1280 pixels. The camera can be triggered and recorded by the outer signal. The photo of the camera and the lens is shown in Figure 4.3 and the details of the camera shows in Table 4.1.

The continuous laser system was used to illuminate the measuring section made by KATO LOKEN, which shows in Figure 4.4. The laser is connected by a special wire. When we turn the laser system on, we can use the laser head to adjust the laser direction and the thickness of laser sheet, of course the magnitude of laser can also be adjusted by the laser system.

The tank used to save water or CMC solution whose size is 150cm\*97cm\*60cm then I used the pumps to deliver the liquid to the flume to consist of a hydraulic circulation system. In my experiments, I used three pumps to deliver the liquid. Two all of them are same, the type of them is CSL-100L, diameter is 25mm, output power is 35L/min. another one is CX-400T, whose diameter is 50mm, output power is 150L/min. Figure 3.8 shows the photo of tank and pumps.

As I discussed in the former part, I used PIV method to depict the velocity field of the flow in the flume. Therefore, it is clear to know that from the principle of PIV, it is an indirect way to obtain the velocity of particle rather than the velocity of fluid. So, the quality of tracer particles play an important role to the results. The proper tracer particle must be large enough

to be visible, appropriate weight can be moved with the flow. More importantly, the concentration of the particle must be testing to make sure good image can be obtained by adding proper quantity. Frankly speaking, the concentration of tracer particles should be changed based on different phenomenon and the only way to know the proper concentration of tracer particle is to practice more. In my experiments, the name of tracer particles is HGS Hollow Glass Spheres produced by DANTEC company and its diameter is 10 $\mu$ m. Figure 3.9 shows the photo of tracer particles. In addition, the proper concentration of tracer particles (concentration of tracer particle=weight of tracer particle  $\div$  weight of liquid) is about 0.000003% (200L CMC solution (concentration= 0.1%) needs 0.6g tracer particle and 250L water needs 1.2g tracer particle.)

Table 4.1 Information of the high-speed camera

<b>Camera type</b>	Color 36bit/Mono 12bit
<b>Sensor type</b>	CMOS
<b>Effective resolution</b>	1280 X 1024 (SXGA)
<b>Sensor format</b>	1/1.8 inch
<b>Lens mount</b>	C-Mount
<b>Interface</b>	USB3.0
<b>Shutter speed (exposure time)</b>	minimum 1 $\mu$
<b>Sensitivity</b>	6.8V/lx $\cdot$ s (mono) / 3.4V/lx $\cdot$ s (color)
<b>Power delivery</b>	12pin AC (battery as option) / 12V
<b>Electric requirements</b>	24WW
<b>Body size</b>	73mm X 118mm X 187.4mm
<b>Body weight</b>	1.2kg
<b>Trigger function</b>	start, end, variable, random (TTL & switch)

[http://www.ditect.co.jp/en/camera/has\\_d72.html](http://www.ditect.co.jp/en/camera/has_d72.html)



Figure 4.2 The photo of the pad

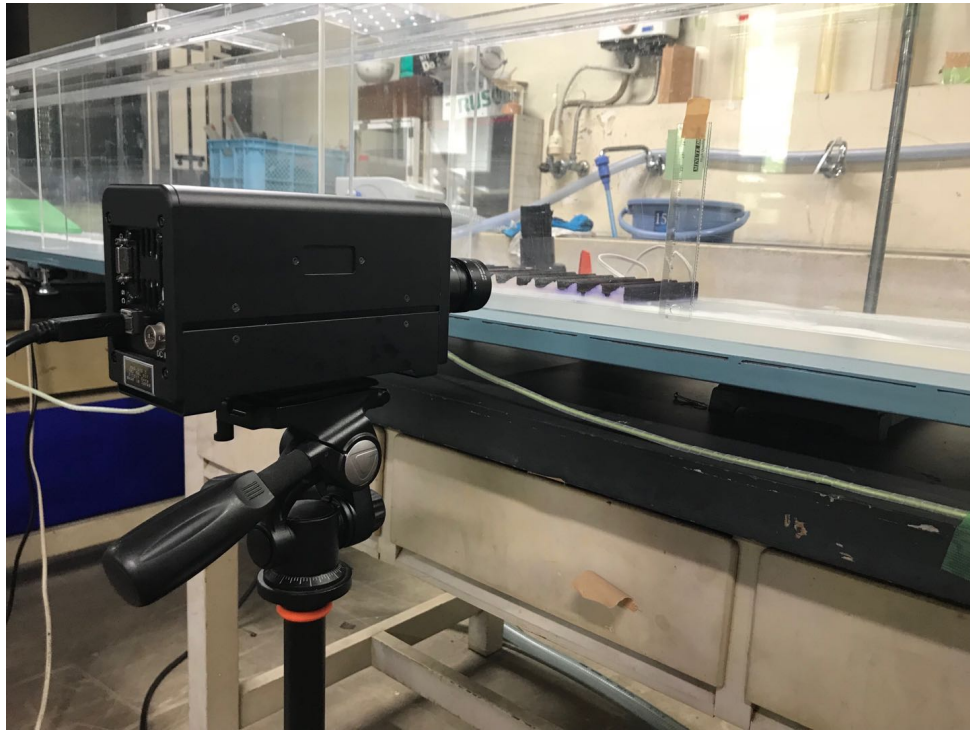


Figure 4.3 The photo of high-speed camera

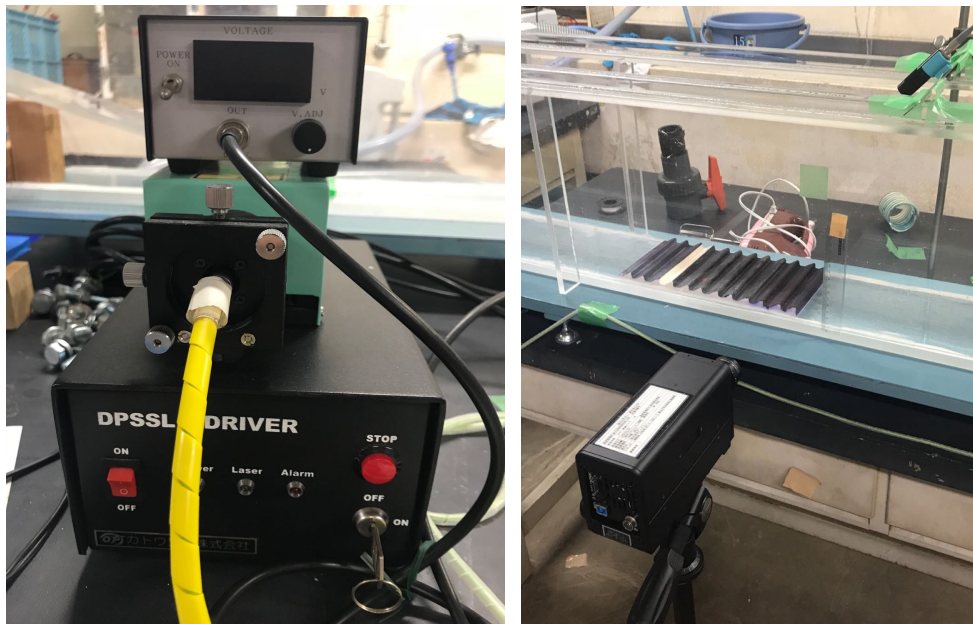


Figure 4.4 The photo of laser system



Figure 4.5 The photo of tank and pumps



Figure 4.6 The photo of tracer particles(HGS, diameter=10 $\mu$ m)

### 4.2.3 Experimental conditions and procedure

The details information about the experimental conditions are shown in Table 4.2 and Table 4.3:

There are totally nine cases in the experiments to simulate different conditions of the real water environment. In each case, the parameters should be calculated by following different similarity law. Firstly, I did the Re-Fr similarity cases then I did the Reynolds similarity cases and Froude similarity cases. The procedure of the experiments is summarized below:

- (1) Mix 250L CMC solution then measure the viscosity of CMC solution by following falling sphere method.
- (2) Make the set-up of the experiment.
- (3) Add tracer particles into the water and mix it to the water then use CCD camera to adjust the concentration of tracer particle.
- (4) Before doing each case, I should measure the velocity of the flow. considering the limitation of experimental equipment, I transfer the velocity measurement to flow discharge measurement. The weight of discharge of the flow equals discharge rate multiply time duration (inner width of the flume is 15cm). The time duration varies from different cases.
- (5) Change the water depth of flume by adjusting the height of the weir, then change the magnitude of the laser. After 5 minutes later, When the water surface is peaceful, I used CCD camera to capture the frames and to save in the fold.

As for the Reynolds similarity law experiment and Froude similarity law case, except the first step, the others are same with Re-Fr similarity law case.

Table 4.2 The derivation between prototype and test model

<i>Case 1</i>	<i>unite</i>	<i>Scale</i>	<i>Scale</i>	<i>Scale</i>
		<i>(Re similarity law)</i>	<i>(Fr similarity law)</i>	<i>(Re –Fr similarity law)</i>
<b>Length scale (<math>L_r</math>)</b>		$L_r$	$L_r$	$L_r$
<b>Velocity (<math>v</math>)</b>	<b>cm/s</b>	$L_v=1/ L_r$	$L_v= v_p L_r^{1/2}$	$L_v= v_p L_r^{1/2}$
<b>Depth (<math>h</math>)</b>	<b>cm</b>	$L_h= L_r$	$L_h= h_p L_r$	$L_h= h_p L_r$
<b>Kinematic viscosity(<math>v</math>)</b>	<b>cm<sup>2</sup>/s</b>	$L_v=1$	$L_v=1$	$L_v=v_p L_r^{3/2}$
<b>Discharge rate(<math>q=h*v</math>)</b>	<b>cm<sup>3</sup>/s/cm</b>	$L_q=1$	$L_q= v_p L_r^{1/2} h_p L_r$	$L_q= v_p L_r^{1/2} h_p L_r$

Table 4.3 Detained information of experimental conditions

<i>Case 1</i>	<i>unite</i>	<i>Prototype</i>	<i>Model</i>	<i>Model</i>	<i>Model</i>
			<i>(Re similarity law)</i>	<i>(Fr similarity law)</i>	<i>(Re –Fr similarity law)</i>
<b>Length scale (<math>L_r</math>)</b>			10.00	10.00	10.00
<b>Velocity (<math>v</math>)</b>	<b>cm/s</b>	0.40	0.04	1.26	1.26
<b>Depth (<math>h</math>)</b>	<b>cm</b>	1.00	10.00	10.00	10.00
<b>Kinematic viscosity(<math>v</math>)</b>	<b>cm<sup>2</sup>/s</b>	0.01	0.01	0.01	0.32
<b>Discharge rate(<math>q=h*v</math>)</b>	<b>cm<sup>3</sup>/s/cm</b>	0.40	0.40	12.65	12.65
<b>Re</b>	<b>m</b>	40.00	40.00	1264.91	40.00
<b>Fr</b>		0.01	0.0004	0.01	0.01
<i>Case 2</i>		<i>Prototype</i>	<i>Model</i>	<i>Model</i>	<i>Model</i>
			<i>(Re similarity law)</i>	<i>(Fr similarity law)</i>	<i>(Re –Fr similarity law)</i>
<b>Length scale (<math>L_r</math>)</b>			10.00	10.00	10.00
<b>Velocity (<math>v</math>)</b>	<b>cm/s</b>	2.00	0.20	6.32	6.32
<b>Depth (<math>h</math>)</b>	<b>cm</b>	1.00	10.00	10.00	10.00
<b>Kinematic viscosity(<math>v</math>)</b>	<b>cm<sup>2</sup>/s</b>	0.01	0.01	0.01	0.32
<b>Discharge rate(<math>q=h*v</math>)</b>	<b>cm<sup>3</sup>/s/cm</b>	2.00	2.00	63.25	63.25
<b>Re</b>		200.00	200.00	6324.56	200.00
<b>Fr</b>		0.06	0.0020	0.06	0.06
<i>Case 3</i>		<i>Prototype</i>	<i>Model</i>	<i>Model</i>	<i>Model</i>
			<i>(Re similarity law)</i>	<i>(Fr similarity law)</i>	<i>(Re –Fr similarity law)</i>
<b>Length scale (<math>L_r</math>)</b>			10.00	10.00	10.00
<b>Velocity (<math>v</math>)</b>	<b>cm/s</b>	4.00	0.40	12.65	12.65
<b>Depth (<math>h</math>)</b>	<b>cm</b>	1.00	10.00	10.00	10.00
<b>Kinematic viscosity (<math>v</math>)</b>	<b>cm<sup>2</sup>/s</b>	0.01	0.01	0.01	0.32
<b>Discharge rate(<math>q=h*v</math>)</b>	<b>cm<sup>3</sup>/s/cm</b>	4.00	4.00	126.49	126.49
<b>Re</b>		400.00	400.00	12649.11	400.00
<b>Fr</b>		0.13	0.0040	0.13	0.13

#### 4.3.4 Data processing

As I shown in Table 4.3, I have three groups: Re similarity groups, Froude groups and Re-Fr similarity groups. In each group there are three different conditions, therefore, I have totally 9 cases. In each case, I have more than 4500 frames of Re-Fr similarity cases and more than 6000 frames of Reynolds similarity law cases and Froude similarity law cases. The frame rate of each case changed from 1/100s to 1/1000s based on the velocity of the flow. Normally, the higher velocity the smaller frame rates will be used in the experiments.

One frame of the Reynolds similarity law case shows in Figure 4.7 and its velocity fields shows in Figure 4.8. The green arrows show the displacement of the flow and saved in Matlab programs, which must reflect the movement of the flow properly and completely. Therefore, plenty of preparation work must be done before getting the appropriate velocity fields.

After depicting the velocity fields of flow. I can get the coordinate values and velocity values of the green arrows in horizontal and vertical directions, respectively. Then, I outputted these datasets to transfer the image scale into geometric scale, then transfer the model scale to prototype scale to make a comparison among Reynolds similarity case, Froude similarity case and Re-Fr similarity case by drawing the velocity profile figures.

.

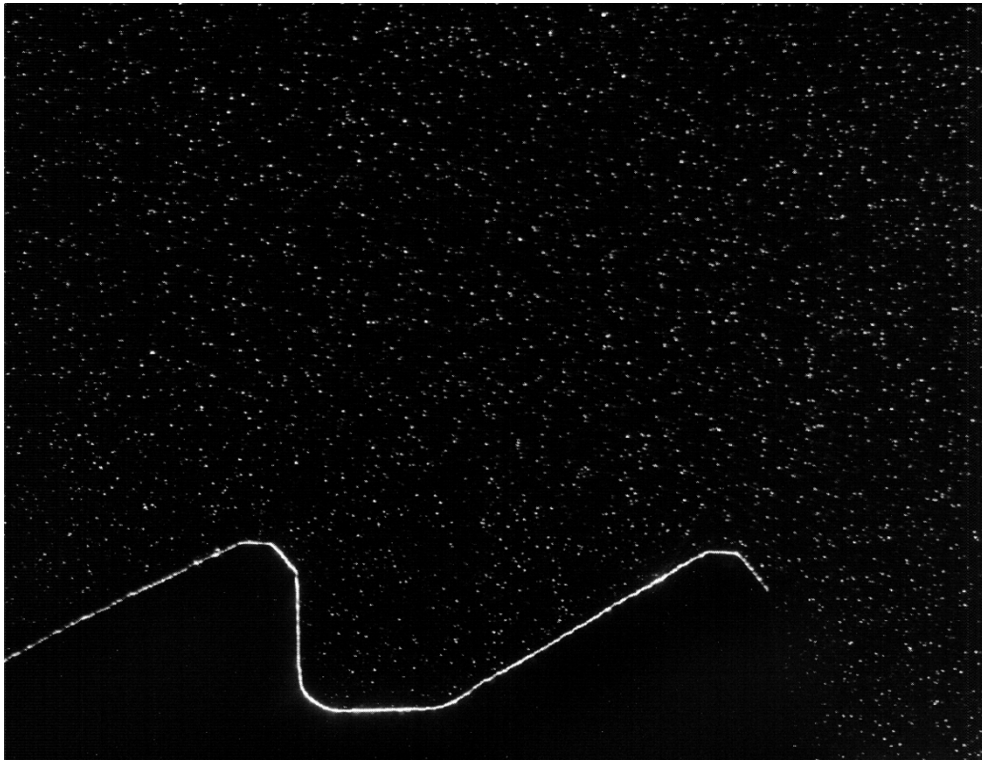


Figure 4.7 Original photo captured by high-speed camera under Reynolds similarity law condition 2 ( $Re=200$ ,  $Fr=0.02$ , Velocity= $0.2\text{cm/s}$ )

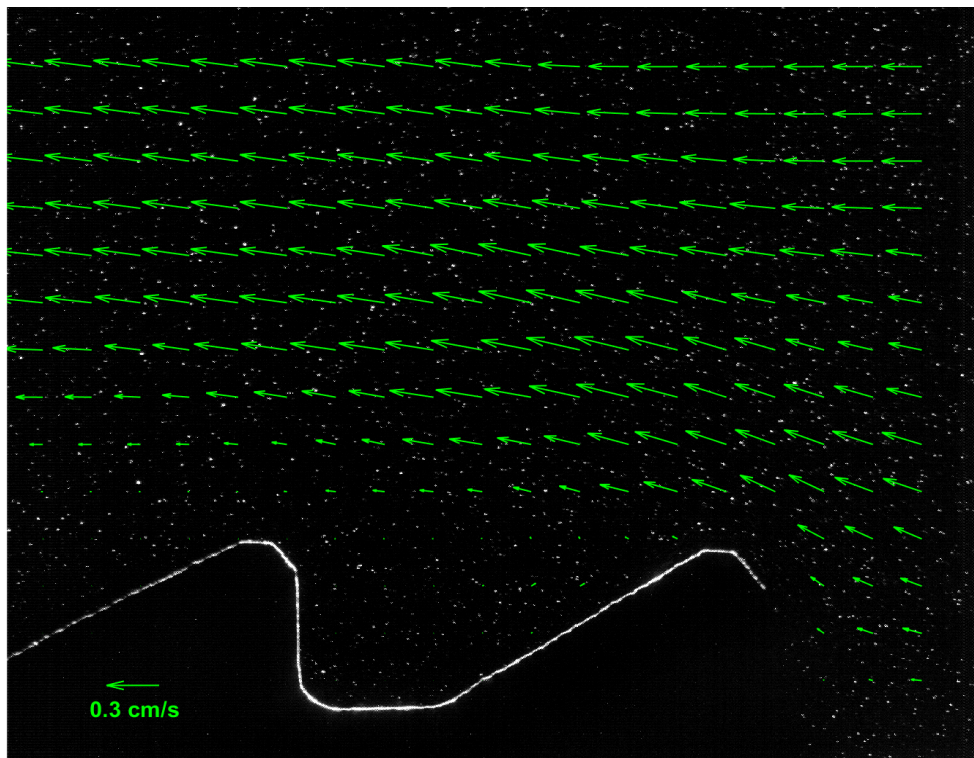


Figure 4.8 The velocity field of Reynolds similarity law condition 2 ( $Re=200$ ,  $Fr=0.02$ , Velocity= $0.2\text{cm/s}$ )

## 4.3 Results

The relationship between average velocity of u-component (horizontal direction) and vertical position (where  $z=0$  is the bottom of the brick) are shown from Figure 4.9 to Figure 4.17 And the Velocity profile by following similarity laws in different condition and position shows from Figure 4.18 to Figure 4.32.

From the above figure, following findings were made

1. In the same condition and the same similarity law cases, the different positions of the roughness elements bring variable velocity values
2. In the same condition and the different similarity law cases, the velocity value of the Reynolds similarity law is the largest one, but the velocity value of the Re-Fr similarity law changed with the increase of the velocity, the velocity values of the Re-Fr are not the smallest one and become bigger than the values of Froude similarity law.
3. The type of the roughness elements changes the velocity fields and the thickness of the boundary layer of the liquid.

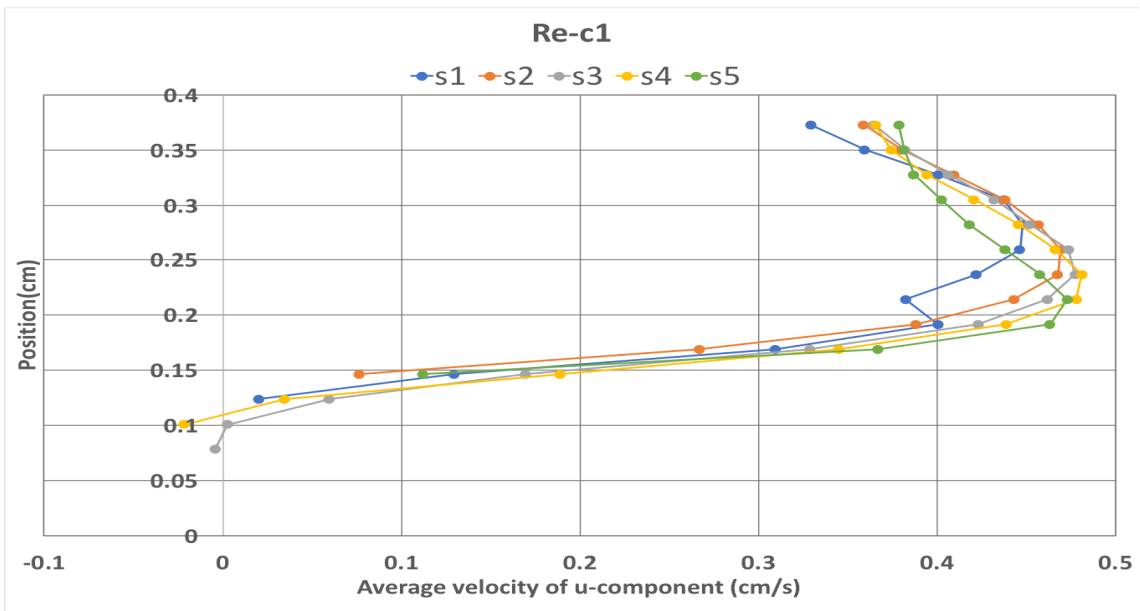


Figure.4.9 The relationship between average velocity of u-component and vertical position  
( $Re=40$ ,  $Fr=0.0004$ ,  $Velocity=0.04\text{cm/s}$ )

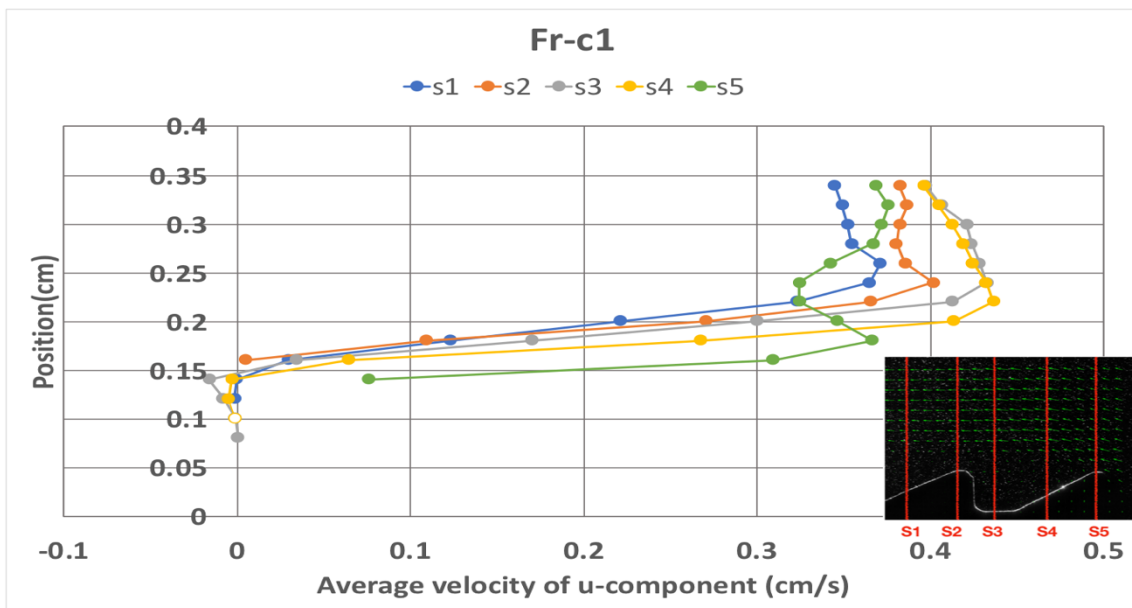


Figure.4.10 The relationship between average velocity of u-component and vertical position  
( $Re=1264.91$ ,  $Fr=0.013$ ,  $Velocity=1.26\text{cm/s}$ )

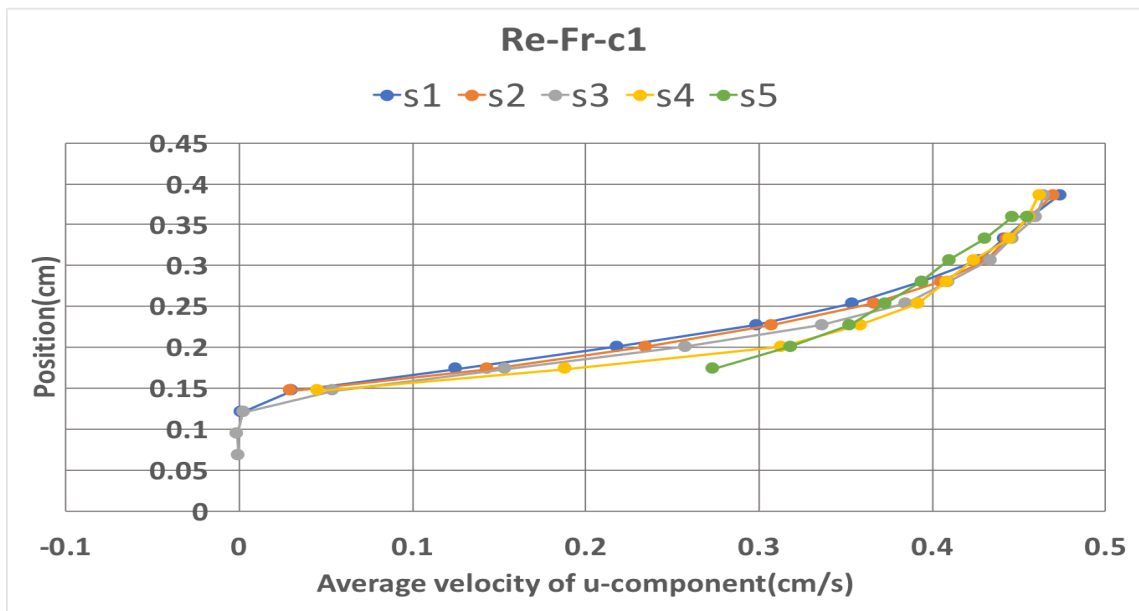


Figure.4.11 The relationship between average velocity of u-component and vertical position (Re=40, Fr=0.013, Velocity=1.26cm/s)

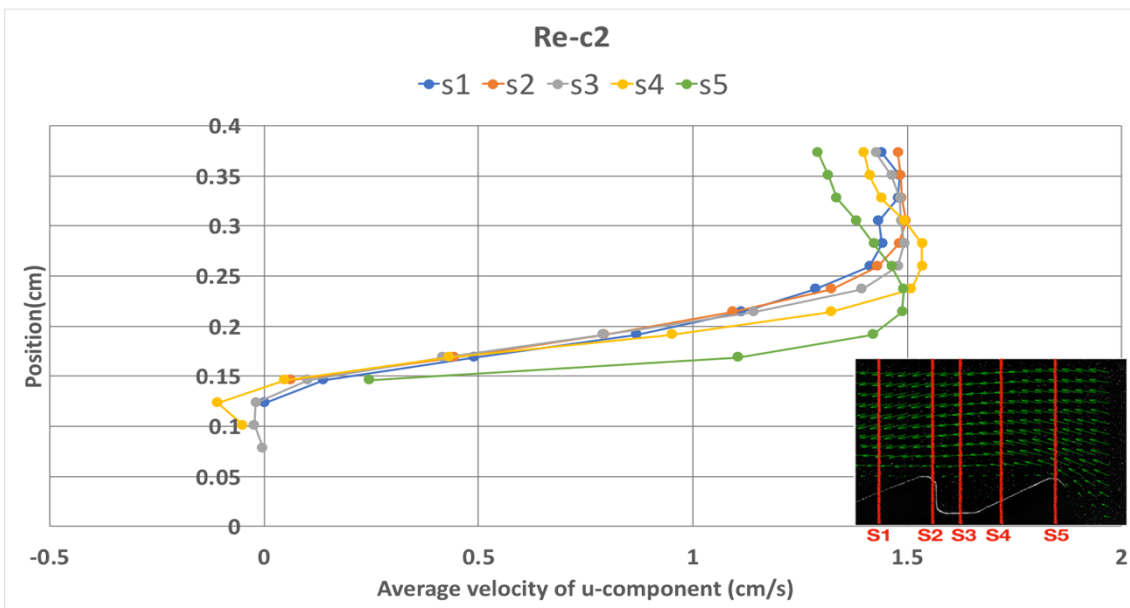


Figure.4.12 The relationship between average velocity of u-component and vertical position (Re=200, Fr=0.002, Velocity=0.2cm/s)

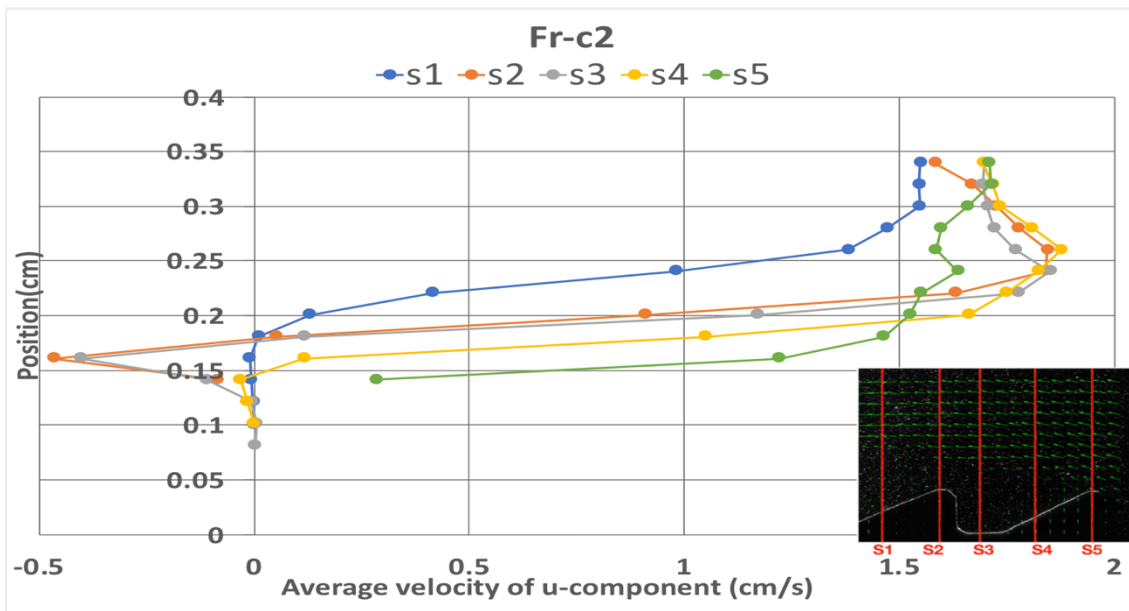


Figure.4.13 The relationship between average velocity of u-component and vertical position ( $Re=6324.56$ ,  $Fr=0.063$ ,  $Velocity=6.32\text{cm/s}$ )

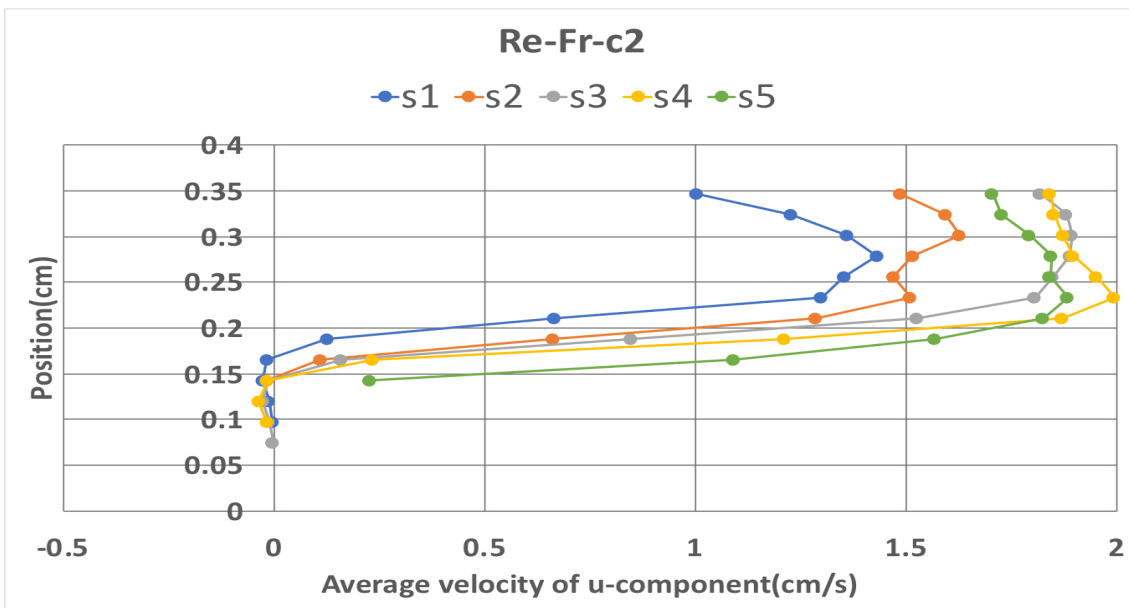


Figure.4.14 The relationship between average velocity of u-component and vertical position ( $Re=200$ ,  $Fr=0.063$ ,  $Velocity=6.32\text{cm/s}$ )

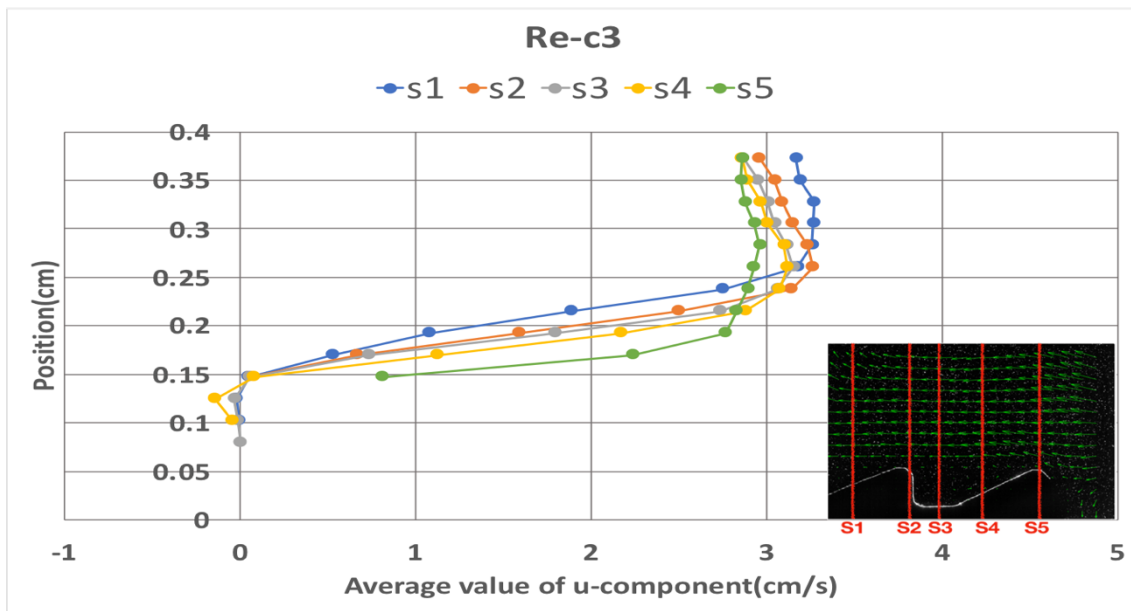


Figure. 4.15 The relationship between average velocity of u-component and vertical position ( $Re=400$   $Fr=0.004$ , Velocity=0.4cm/s)

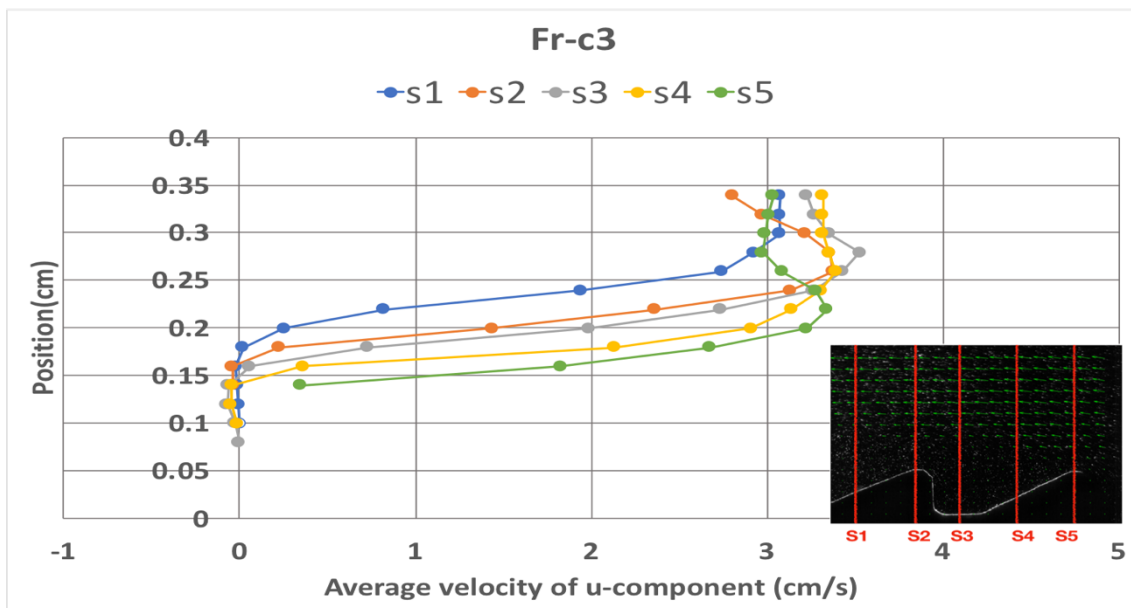


Figure.4.16 The relationship between average velocity of u-component and vertical position ( $Re=12649.11$   $Fr=0.126$ , Velocity=12.65cm/s)

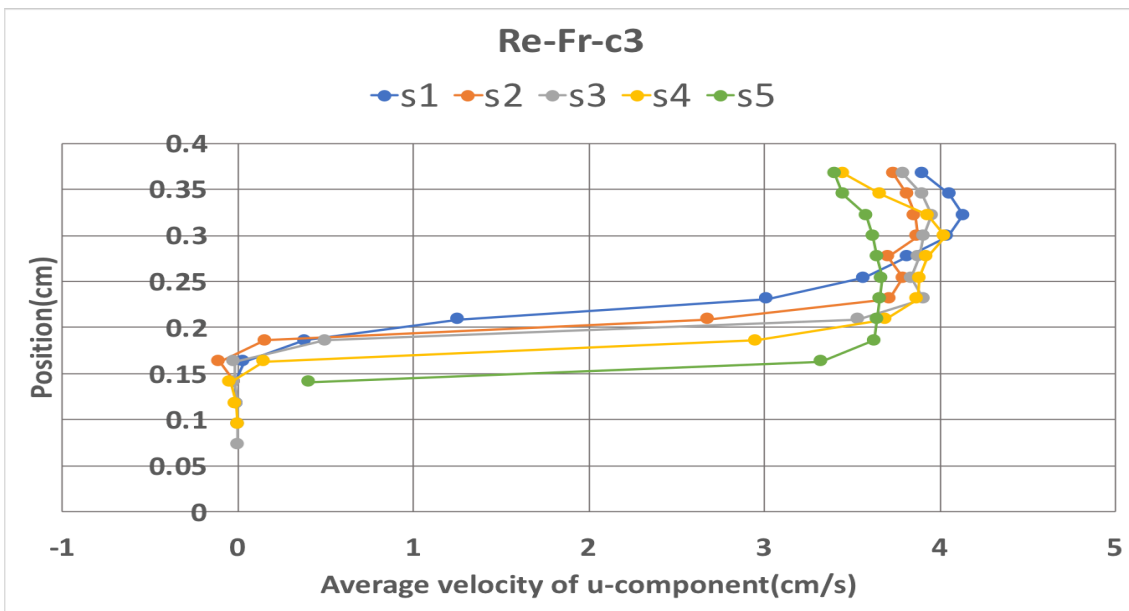


Figure.4.17 The relationship between average velocity of u-component and vertical position (Re=400 Fr=0.126, Velocity=12.65cm/s)

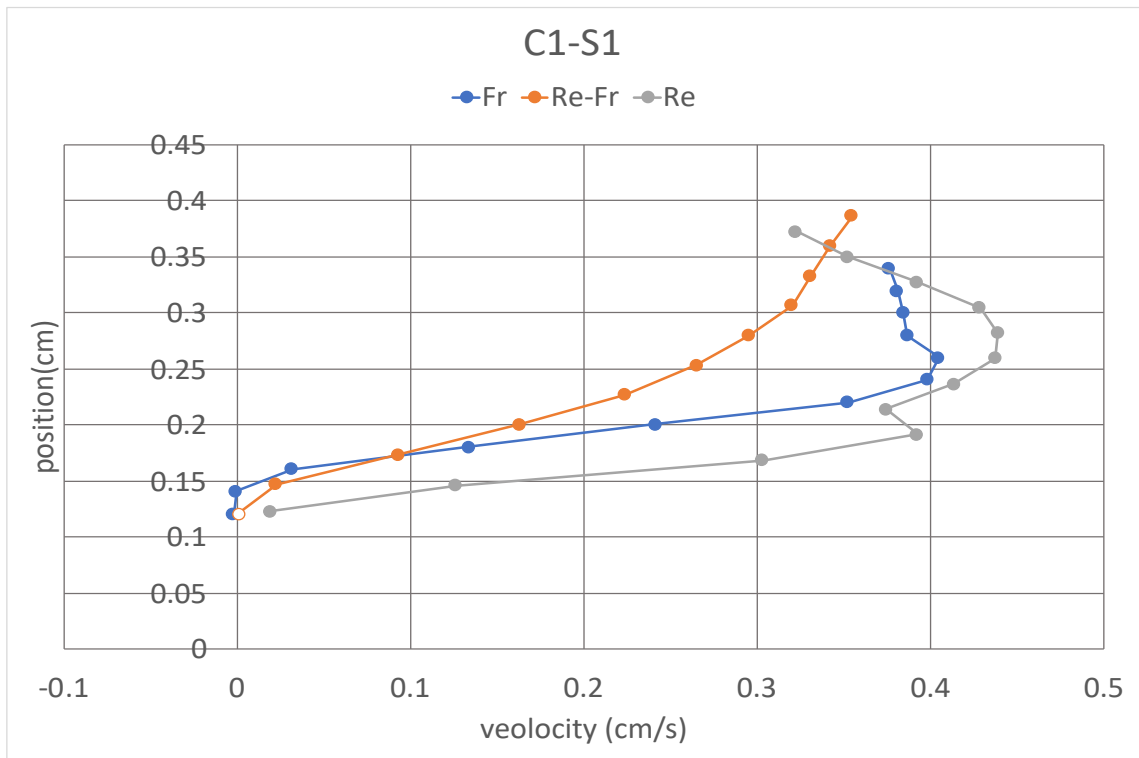


Fig.4.18 Velocity profile by following Re,Fr,Re-Fr similarity law in condition 1, section 1

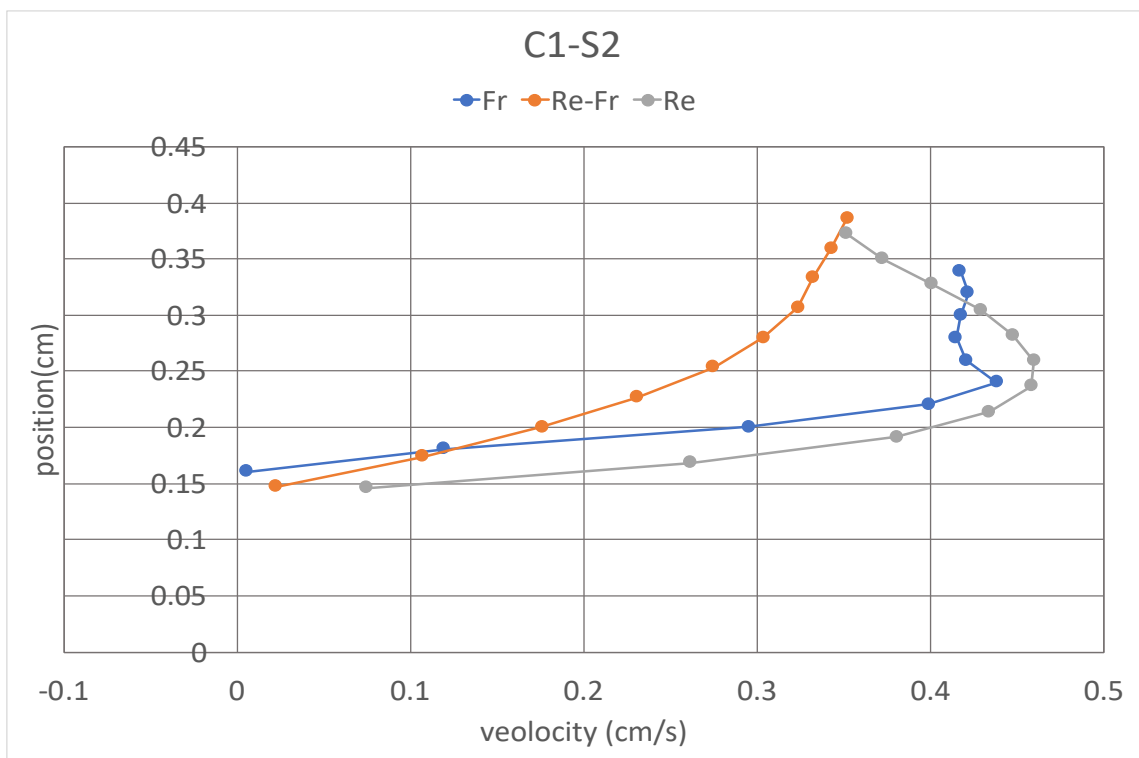


Fig.4.19 Velocity profile by following Re,Fr,Re-Fr similarity law in condition 1, section 2

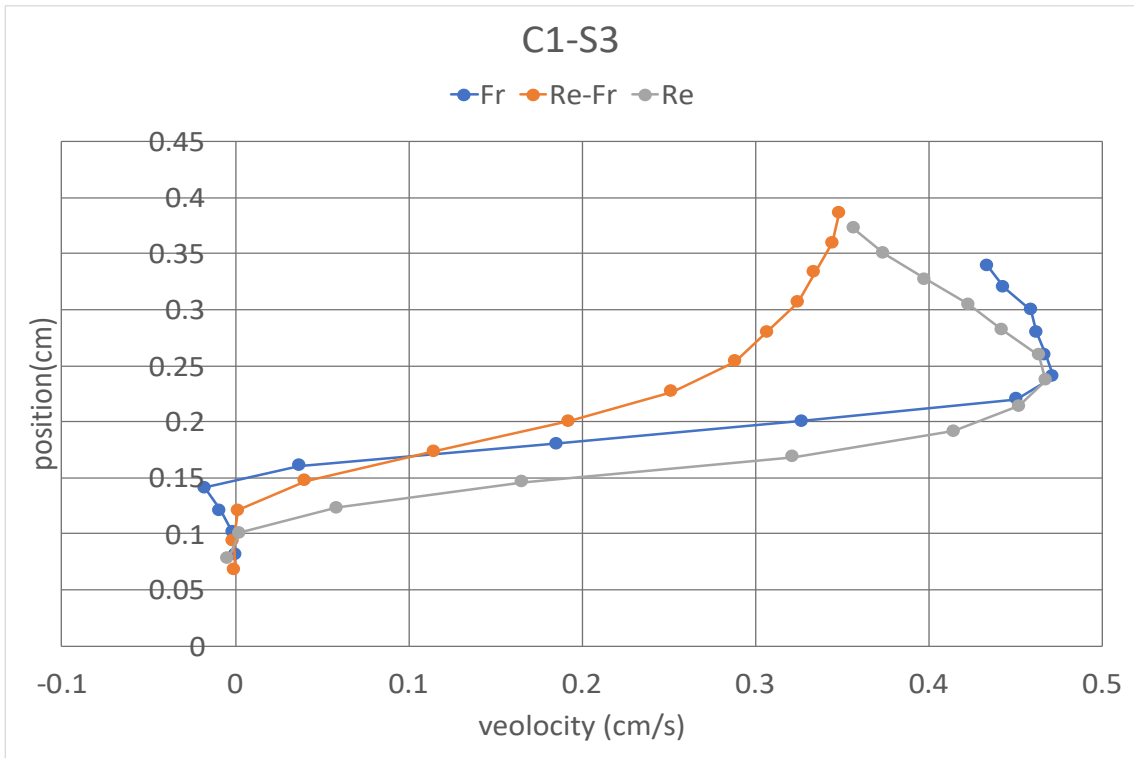


Fig.4.20 Velocity profile by following Re,Fr,Re-Fr similarity law in condition1, section 3

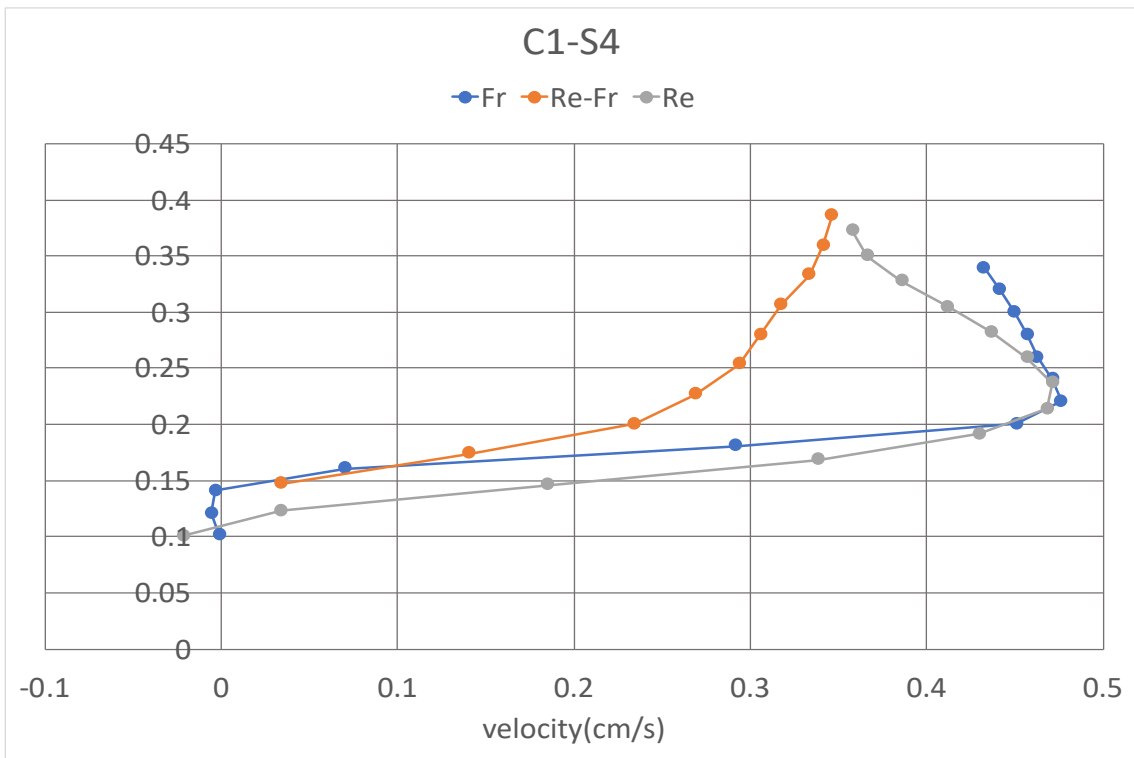


Fig.4.21 Velocity profile by following Re,Fr,Re-Fr similarity law in condition 1, section 4

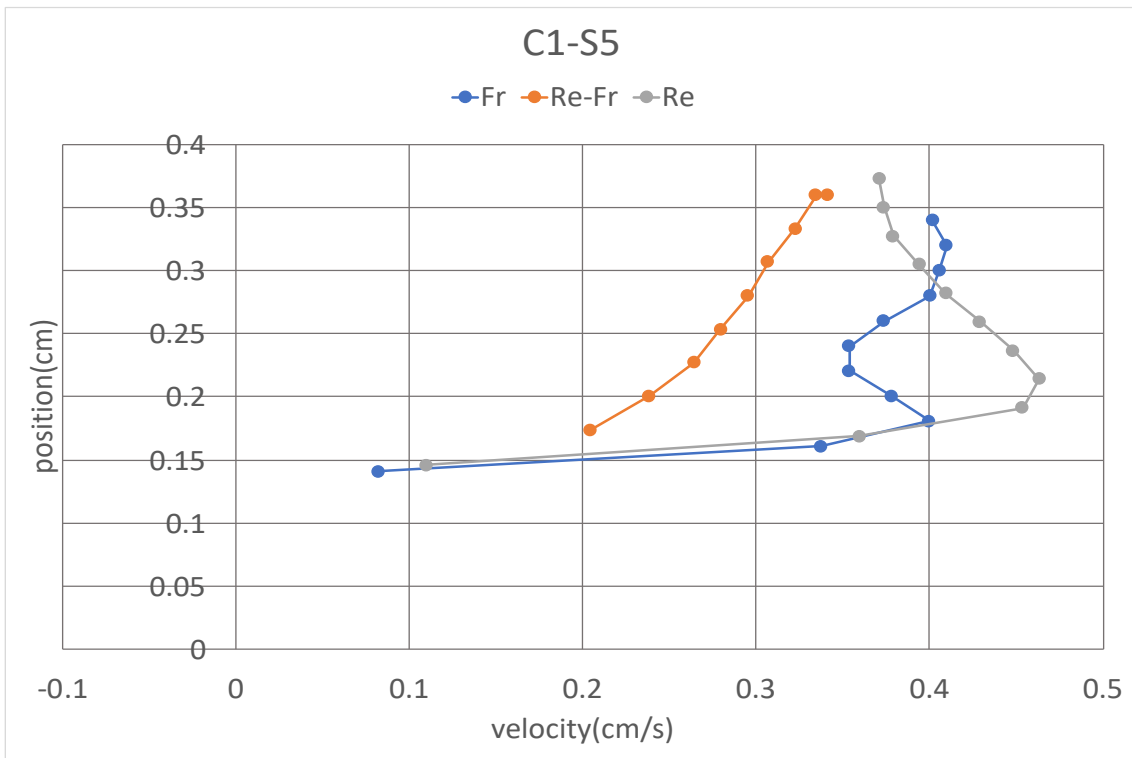


Fig.4.22 Velocity profile by following Re,Fr,Re-Fr similarity law in condition 1, section 5

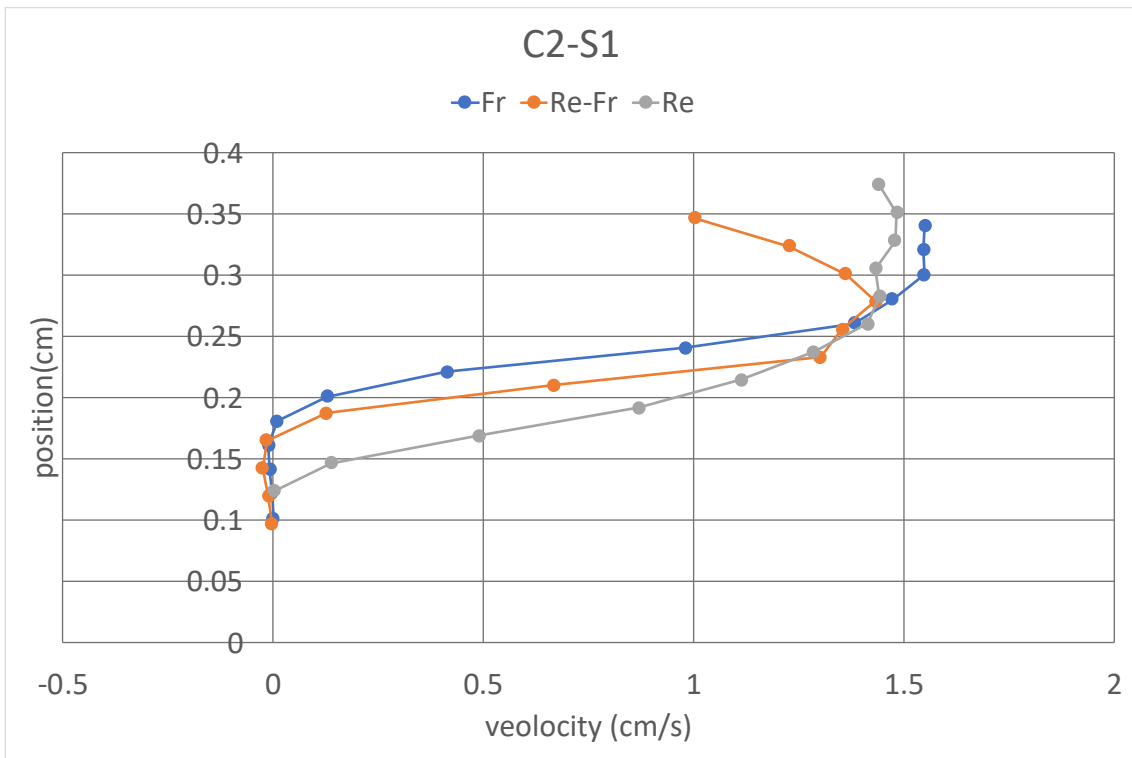


Fig.4.23 Velocity profile by following Re,Fr,Re-Fr similarity law in condition 2, section 1

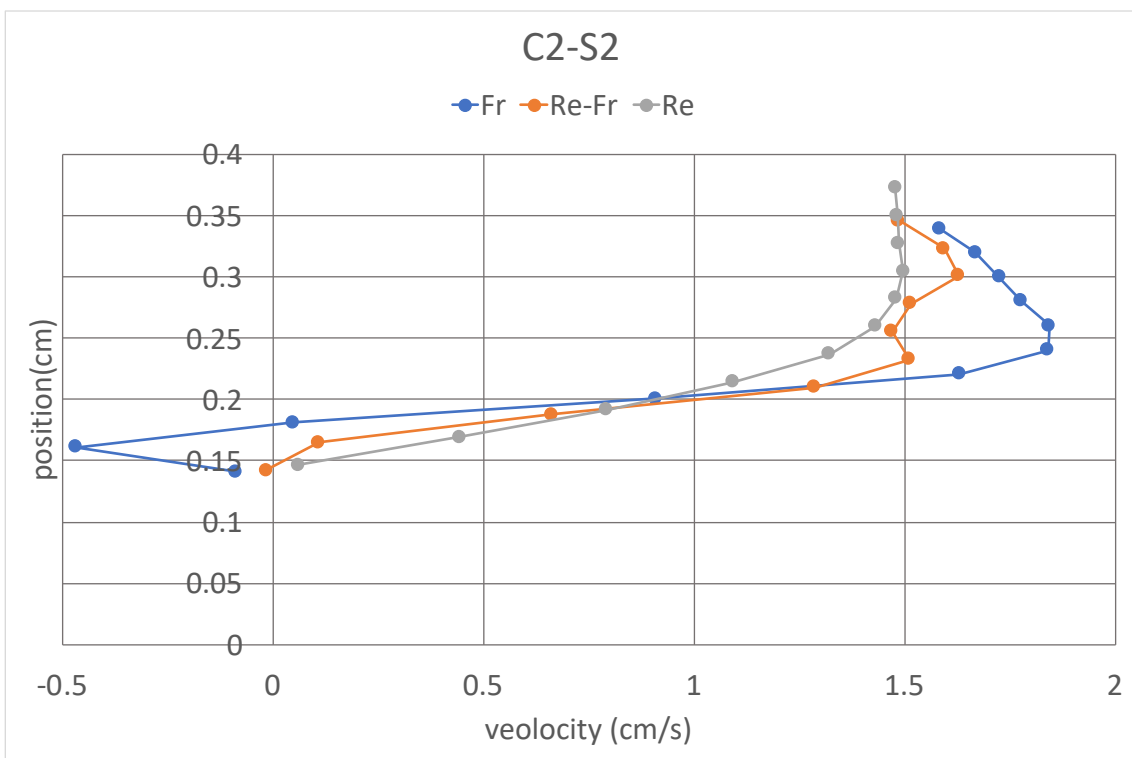


Fig.4.24 Velocity profile by following Re,Fr,Re-Fr similarity law in condition 2, section 2

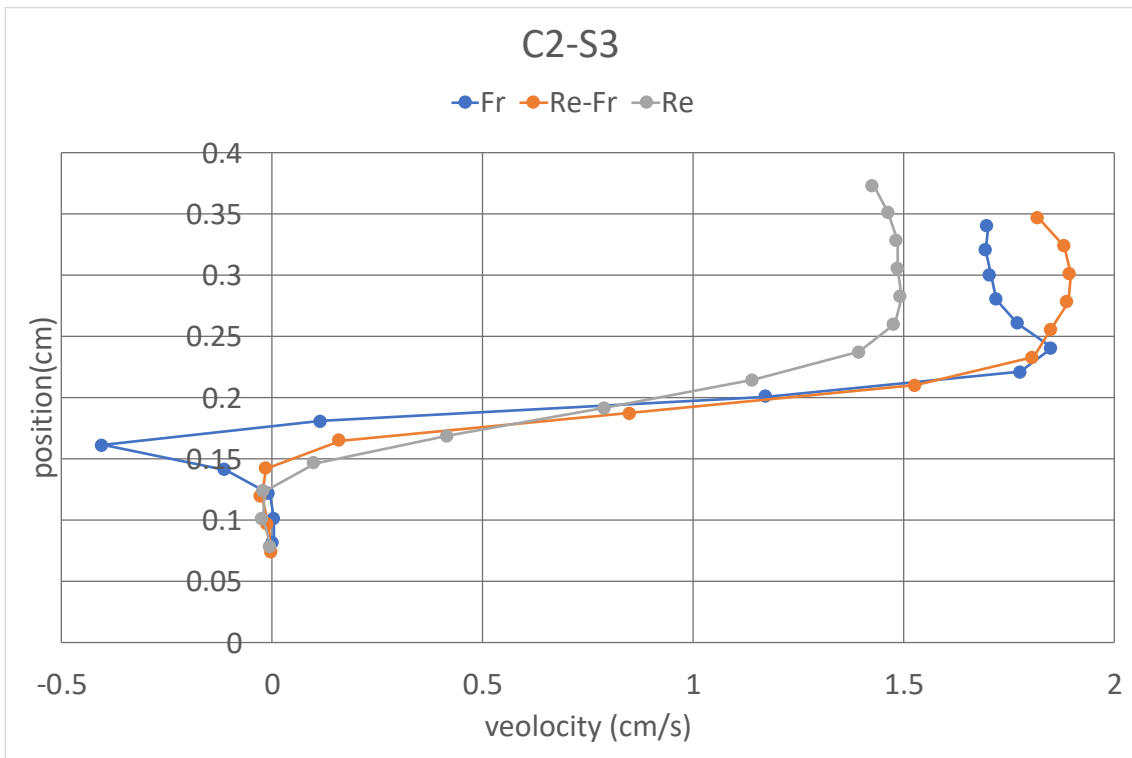


Fig.4.25 Velocity profile by following Re,Fr,Re-Fr similarity law in condition 2, section 3

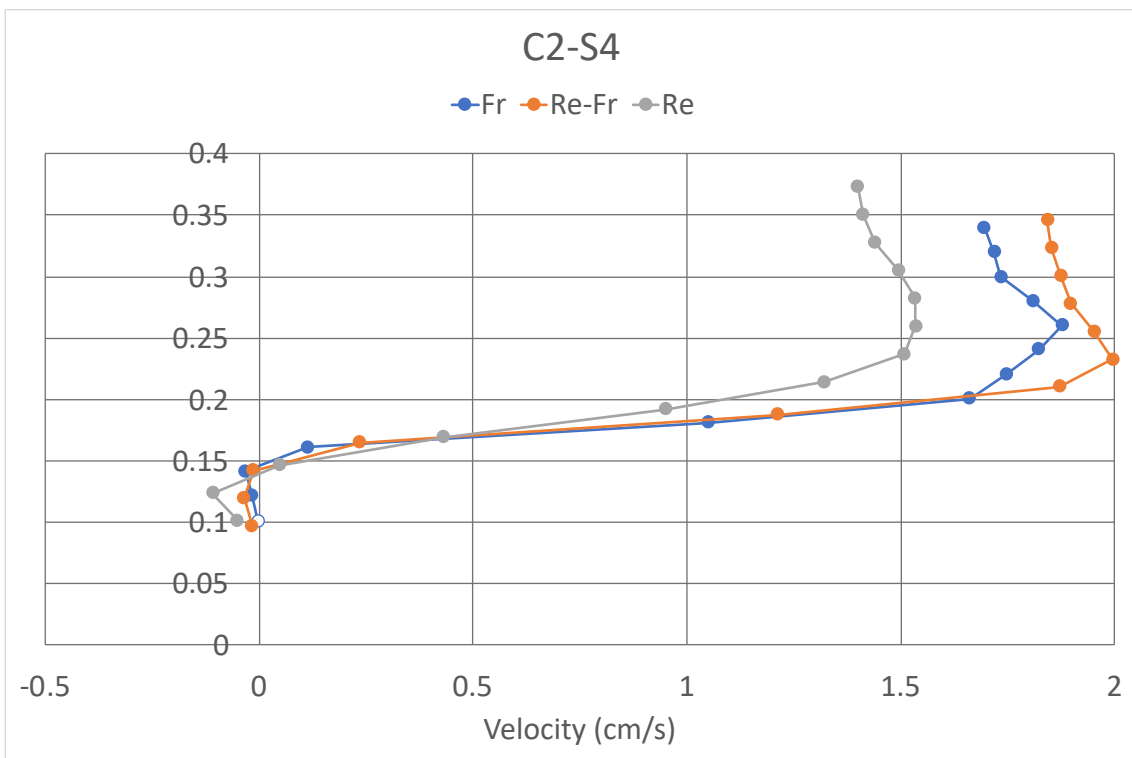


Fig.4.26 Velocity profile by following Re,Fr,Re-Fr similarity law in condition 2, section 4

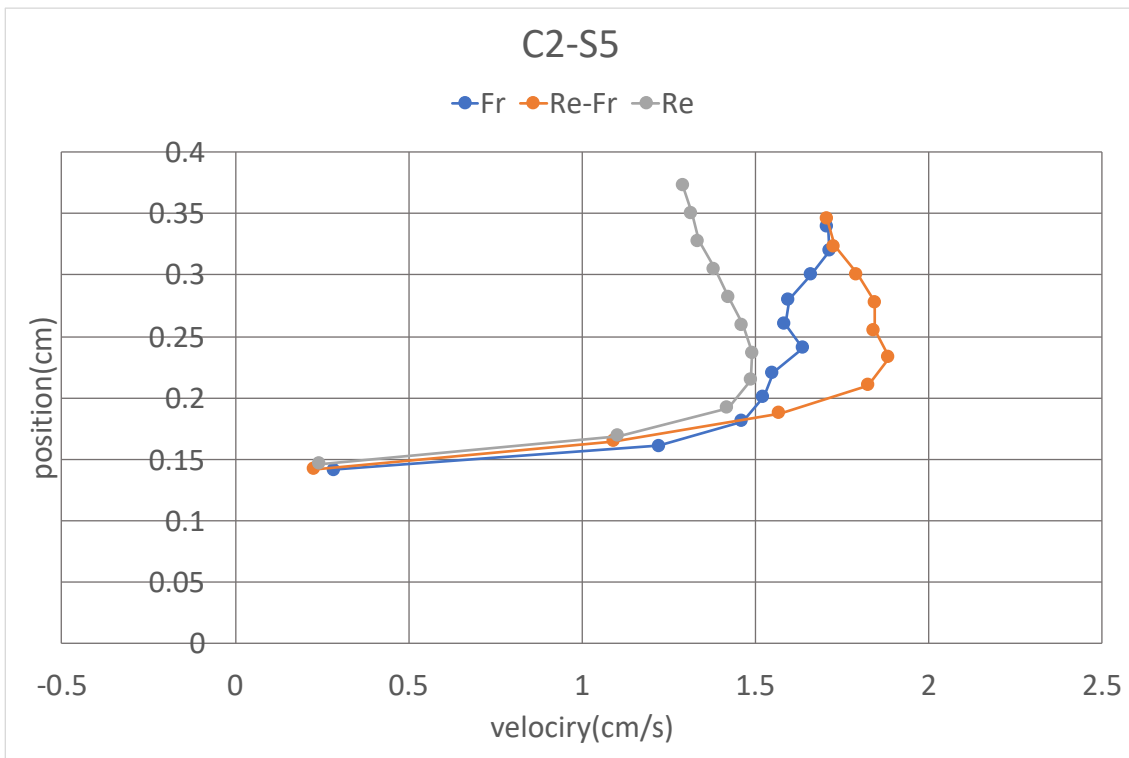


Fig.4.27 Velocity profile by following Re,Fr,Re-Fr similarity law in condition 2, section 5

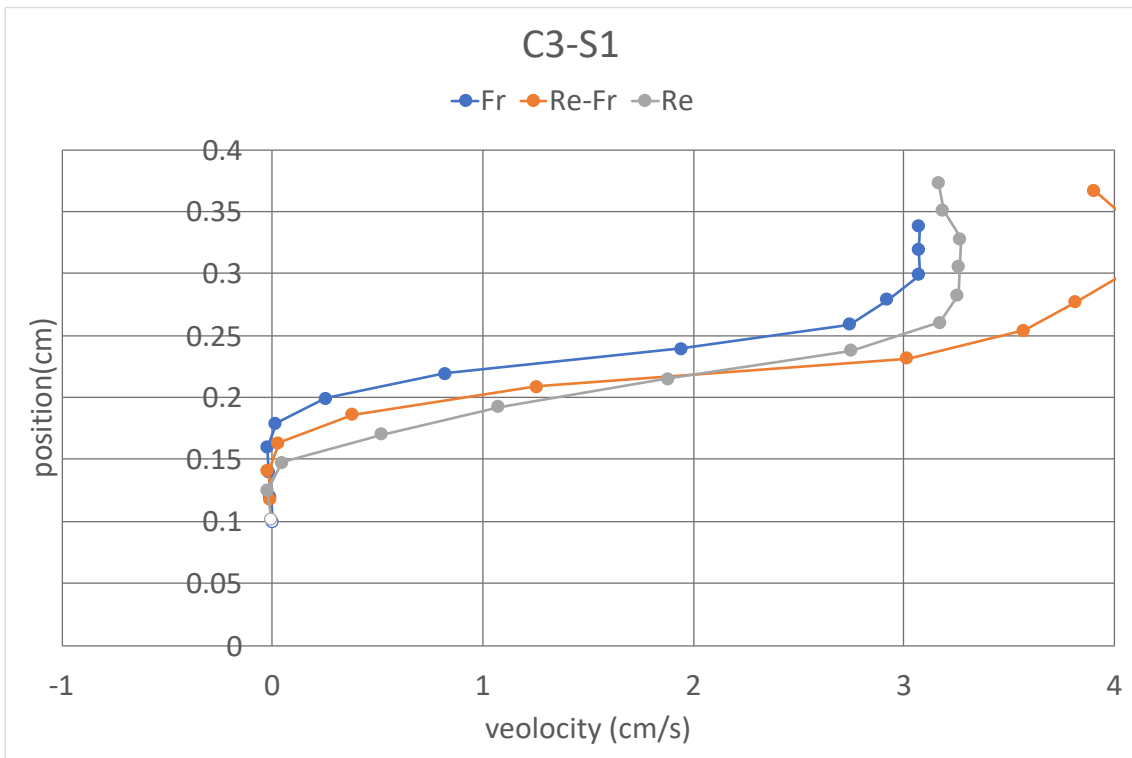


Fig.4.28 Velocity profile by following Re,Fr,Re-Fr similarity law in condition 3, section 1

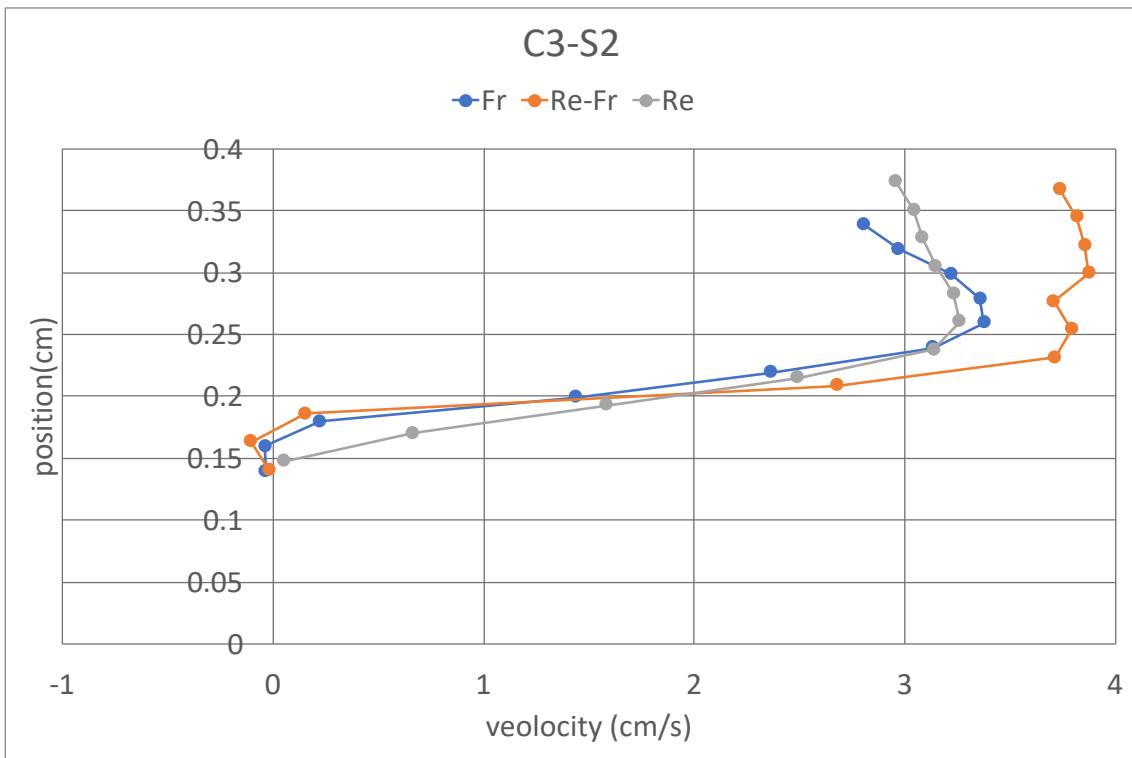


Fig.4.29 Velocity profile by following Re,Fr,Re-Fr similarity law in condition 3, section 2

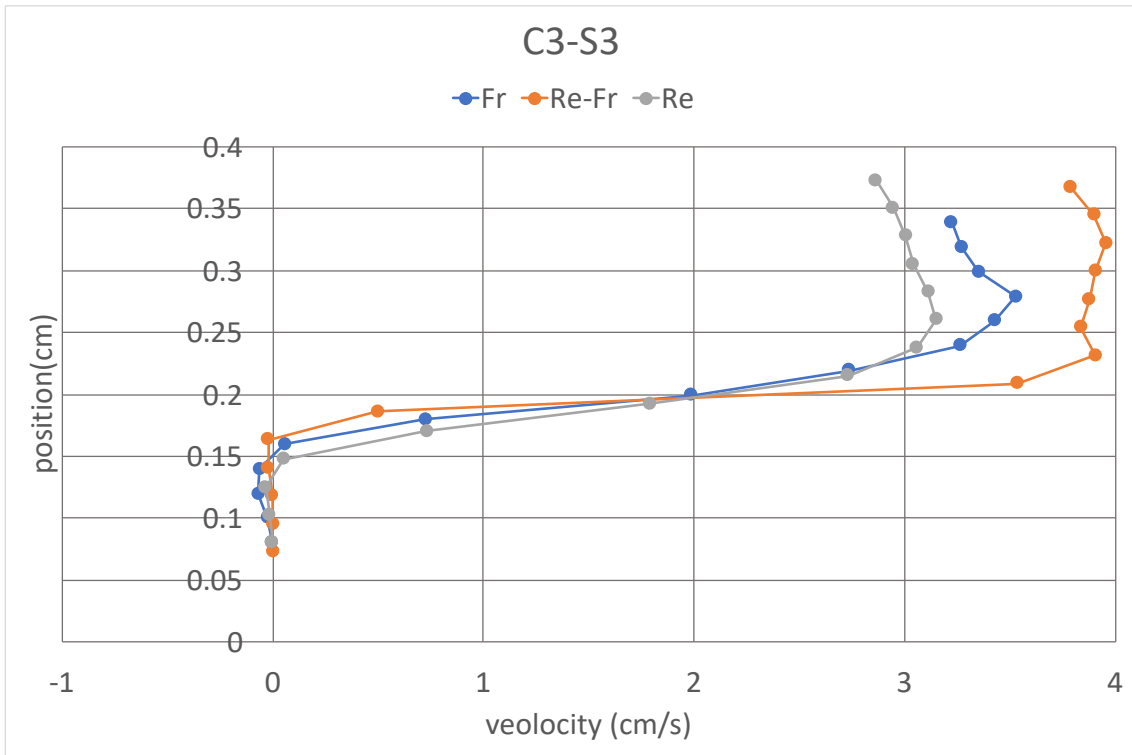


Fig.4.30 Velocity profile by following Re,Fr,Re-Fr similarity law in condition 3, section 3

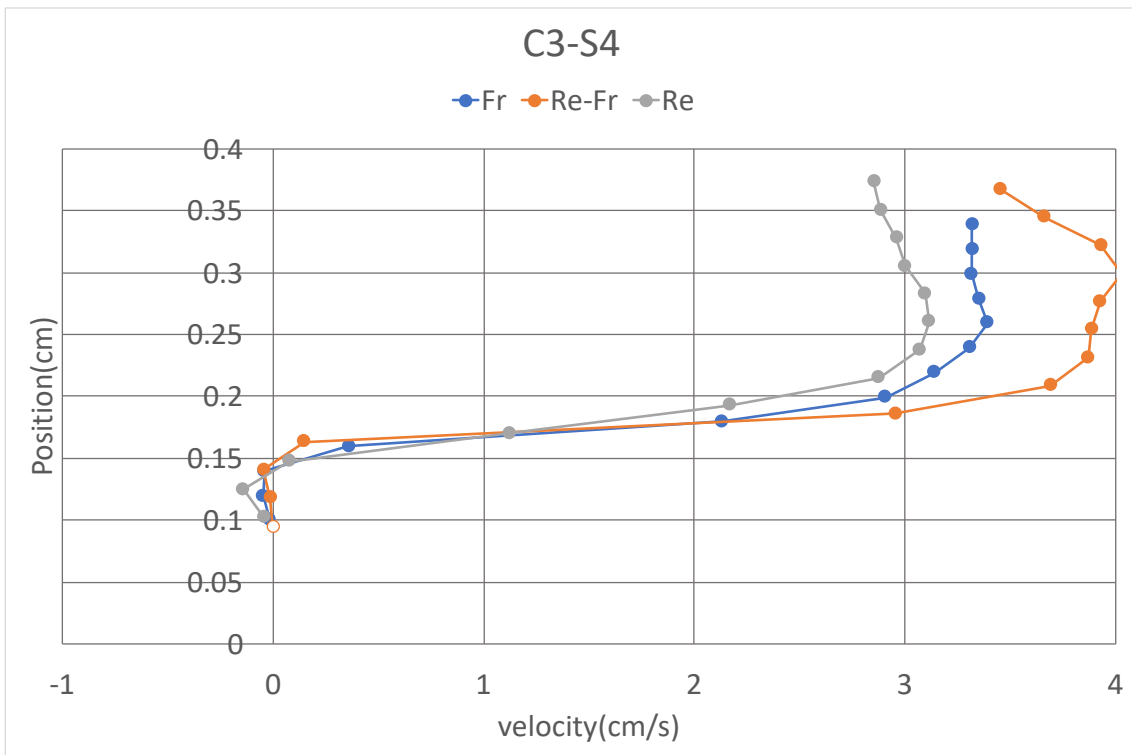


Fig.4.31 Velocity profile by following Re,Fr,Re-Fr similarity law in condition 3, section 4

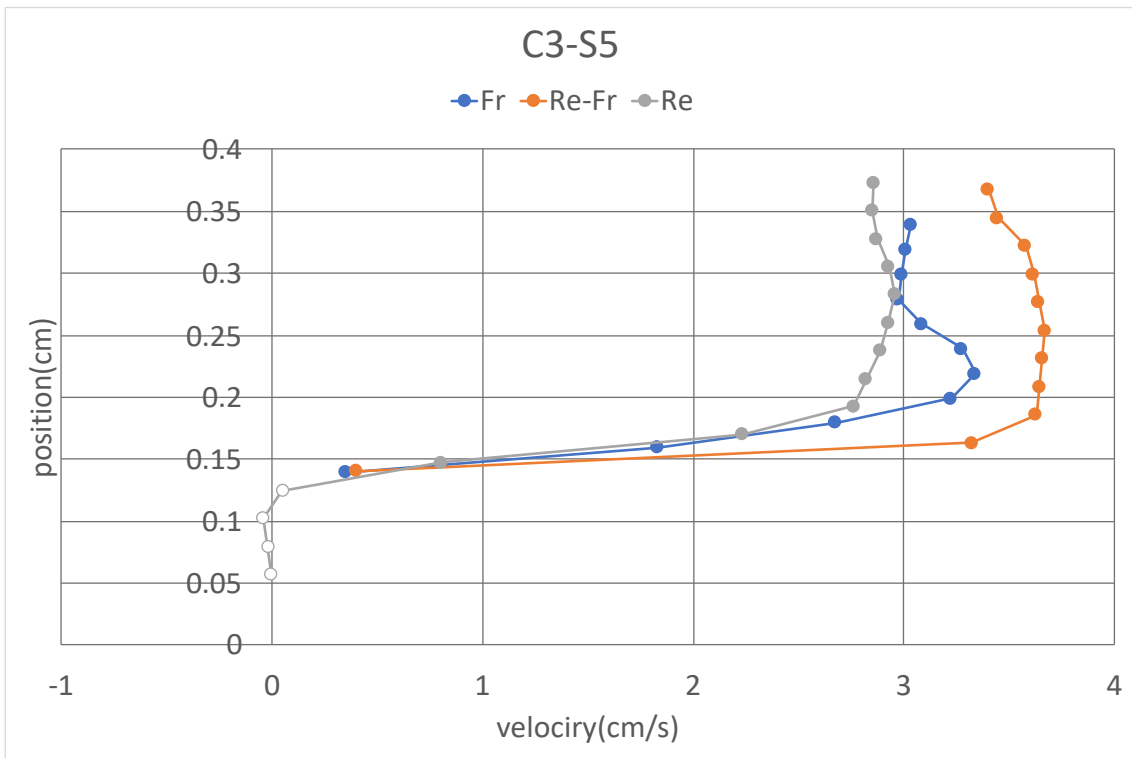


Fig.4.32 Velocity profile by following Re,Fr,Re-Fr similarity law in condition 3, section 5

## 4.4 Discussion and conclusion

From the above figures, the following conclusion can be drawn.

1. The tendency of the flow fields and the thickness of boundary layer around the roughness element are similar but details are different by observing the flow fields over small roughness elements.
2. Velocity gradient and boundary layer thickness effected by different similarity law  
Bigger  $Re$  gives smaller velocity gradient and thicker boundary layer  
Bigger  $Fr$  gives bigger velocity gradient and thinner boundary layer
3. Vortex flow:  
In crest areas, vortex flow only appears in  $Re$ - $Fr$  and  $Fr$  similarity law cases.  
In the trough areas, the return flow appears in all cases.

## Chapter 5: Conclusions and limitations

The conclusions can be drawn as follows:

1. The relationship between the kinematic viscosity and concentration of CMC solution follows:

$$\nu_{cmc} = \nu_{water} \times (1 + 4.5 \times 10^8 \times C_{cmc}^{2.4})$$

2. The tendency of the flow fields and the thickness of boundary layer around the roughness element are similar among different similarity law but details are different.
3. Velocity gradient and boundary layer thickness are affected by the similarity laws.  
Bigger Reynolds value gives smaller velocity gradient and thicker boundary layer  
Bigger Froude value gives bigger velocity gradient and thinner boundary layer.
4. Vortex flow:

In crest areas, vortex flow only appears in Re-Fr and Fr similarity law cases.

In the trough areas, the return flow appears in all cases.

While doing experiments the limitations are as follows:

1. Temperature is an important factor to influence the viscosity of CMC solutions but in the whole experiments, I didn't pay much attention on this influential factor
2. To find the difference among different similarity laws, if we provide different length scale will be better.
3. The prototype experiment should also be conducted to help us make a clear comparison among each similarity law case.

.

## **Acknowledgment**

Time goes by, two years post-graduate study will be finished soon. I really appreciated to all of you who contributed in my academic work and daily life.

First and foremost, I would like to thank my supervisor, Professor Akio Okayasu, for accepting me into his laboratory to start an amazing Japanese journey. During this two year, I learned a lot from his rigorous academic attitude, elegant behavior and logical thinking. He provided me unforgettable experience in Japan by giving me abundant information focus on research topic, supporting me various activities, and demanding a high quality of work.

Additionally, I would like to thank Professor Tsuyoshi Ikeya who had provided me extremely suggestions and paid a lot of time and attention to my study. His strict academic attitude, patient teaching and kind explanation made deep impression on me and inspired me to improve myself. More importantly, Professor Tsuyoshi Ikeya taught me how to think about problems with engineering thinking and logical thinking. Acknowledgement also to Professor Kazuo Tani, and Associate Professor Daisuke Inazu for their advices in my work.

Furthermore, I greatly benefited from Doctor Dejun Feng's sophisticated logic. I learned a lot from his concentration on solving practical difficulties, his ability to explain a complex idea to an operable experimental design and his encouragement on experiments and daily life. Even when he graduated from our lab, he also gave me plenty of cherished suggestions.

I also should say thank you to Doctor Wu Lianhui. He helped me a lot to correct my mistakes and I really admired to his knowledge about Japanese language, culture and qualified life styles.

Doctor Wang Yulong, his optimistic, persistence and patient encourage me a lot. Thanks for you to help me choose lectures and give me so much conducive suggestions. Especially, during the graduation period I occupied you so much time to ask the related questions about my master thesis and final defense. Acknowledgement also greet to Mr. Yoshiyuki Uno, Mr. Kitamura Fukutaro, Mr. Du Yugeng, Mr. Chen Tianning, Ms. Nanami Noguchi, Ms. Narumi Konno, Mr. Akihiro Tomita, Mr. Shotaro Suzuki (my tutor who helped me adapt to Japanese life ) Mr. Oyanagi Atsuya, Mr. Otsuka Takatoshi, Mr. Dobashi Yoichiro, Mr. Yoneyama Yuichi, Mr. Hayashi Fumiyasu, Mr. Orita Kiyotaka, Mr. Kitamura Kiminori, Ms. Moe Yu Par Zaw, Ms. Bi Dongxu, Ms. Li Fengying.

I would like to thank the various instructors and members of the JCK program with whom we had memorable friendship in these two years, greetings also give to them who have not already mentioned: Miss. Jin, Miss. Qu, Miss. Shen, Miss. An who gave me kind care in Japan. My program fellows, Mr. Pan Deng, Mr. Cheng Xiangyu, Ms. Yang Fang, Ms. Fang Lu, Mr. Meng Lingcai, Mr. Wang Xin, Mr. Ye Tao, Mr. Gao Qingli and Mr. Wang Cong we spend time together in campus during workshops and courses. They provided a friendly and cooperative atmosphere when we are studying together, useful feedback and insightful comments to my work.

In addition, I am grateful to Zhejiang Ocean University to provide me such kind opportunity to study in Japan. Also, I would like to thank Professor Wang Zhizheng for his kind consideration and help.

Finally, special thanks should be given to my parents for always supporting and encouraging me throughout my education and life.

## References

- Bangalee M Z I, Miao J J, Lin S Y, et al. Flow visualization, PIV measurement and CFD calculation for fluid-driven natural cross-ventilation in a scale model[J]. *Energy and Buildings*, 2013, 66: 306-314.
- Baine M. Artificial reefs: a review of their design, application, management and performance[J]. *Ocean & Coastal Management*, 2001, 44(3-4): 241-259.
- Clayton M N. Propagules of marine macroalgae: structure and development[J]. *British Phycological Journal*, 1992, 27(3): 219-232.
- Dean R G, Dalrymple R A. *Water wave mechanics for engineers and scientists*[M]. World Scientific Publishing Company, 1991.
- Ditton R B, Osburn H R, Baker T L, Thailing C E. Demographics, attitudes, and reef management preferences of sport divers in offshore Texas waters[J]. *ICES Journal of Marine Science*, 2002, 59(suppl): S186-S191.
- Feng Dejun Laboratory observations of turbulence and bed shear stress in the wash zone, 2017
- Feng Dejun Laboratory of bottom boundary layer in the bore-drive swash zone on impermeable slope, 2013
- Hughes S A. *Physical models and laboratory techniques in coastal engineering*[M]. World Scientific, 1993.

- Hassan Y A, Dominguez-Ontiveros E E. Flow visualization in a pebble bed reactor experiment using PIV and refractive index matching techniques[J]. Nuclear Engineering and Design, 2008, 238(11): 3080-3085.
- Jensen A. European artificial reef research network (EARRN): final report and recommendations[J]. University of Southampton, UK, 1998.
- Jiang Z, Liang Z, Zhu L, et al. Numerical simulation of effect of guide plate on flow field of artificial reef[J]. Ocean Engineering, 2016, 116: 236-241.
- Jiang Z, Liang Z, Tang Y, et al. Numerical simulation and experimental study of the hydrodynamics of a modeled reef located within a current[J]. Chinese Journal of Oceanology and Limnology, 2010, 28(2): 267-273.
- Khan W A, Pop I. Boundary-layer flow of a nanofluid past a stretching sheet[J]. International journal of heat and mass transfer, 2010, 53(11-12): 2477-2483.
- Liang Z L, Shi S, Mei J X. Effects on algal density of substrate roughness and sediment, Haiyang Xuebao, 2016, 38(10): 105-112.
- Ludwig Prandtl. Fluid Flow in Very Little Friction. German: The third international congress of mathmagicians in Heidelberg, 1904
- Merzkirch W. Flow visualization[M]. Elsevier, 2012.
- Morrison F A. Data correlation for drag coefficient for sphere[J]. Department of Chemical Engineering, Michigan Technological University, Houghton, MI, 2013.
- Munson B R, Young D F, Okiishi T H, et al. Fundamentals of fluid mechanics. Hoboken[J]. John Wiley & Sons, Inc, 2006, 69: 520.

Makinde O D, Aziz A. Boundary layer flow of a nanofluid past a stretching sheet with a convective boundary condition[J]. *International Journal of Thermal Sciences*, 2011, 50(7): 1326-1332.

Price S J, Sumner D, Smith J G, et al. Flow visualization around a circular cylinder near to a plane wall[J]. *Journal of Fluids and Structures*, 2002, 16(2): 175-191.

Raffel M, Willert C E, Scarano F, et al. Particle image velocimetry: a practical guide[M]. Springer, 2007.

Reed, D.C., Brzezinski, M.A., Coury, D.A., Graham, W.M., Petty, R.L., 1999. Neutral lipids in macroalgal spores and their role in swimming. *Mar. Biol.* 133, 737–744.

Relini G. The Loano artificial reef[M]//Artificial reefs in European seas. Springer, Dordrecht, 2000: 129-149.

Shaughnessy E J, Katz I M, Schaffer J P. Introduction to fluid mechanics[M]. New York: Oxford University Press, 2005.

Smits A J. Flow visualization: techniques and examples[M]. World Scientific, 2012.

Shi C, Zhang D, Liang Z L, Mei J X. The effect of substrate roughness and sediment on algal spore attaching ability and sporeling density. *China Academic Journal Electronic Publishing House*, 2014, 2: 118-124.

Seaman Jr W. Frontiers that increase unity; defining an agenda for European artificial reef research[C]//European Artificial Reef Research Network (EARRN) Conference, European Community Specific Programme for Research, Technological Development and Demonstration in the Field of Agriculture and Agro-Industry, Including Fisheries. 1996: 26-30.

Tang Y, Long X, Wang X, Jiang Z Y, Cheng H, Zhang T Z. Comparative analysis on flow field effect of general artificial reefs in China[J]. Transactions of the Chinese Society of Agricultural Engineering, 2017, 33(8): 97-103.

Tsumura K, Kakimoto H, Noda M. The history and future of artificial reefs and related aquatic habitats in Japan[J]. Proceedings 7th CARAH, 1999, 1: 264-271.

Wang Yulong, Research on submerged inclined plate breakwater for wave control,2017

Zhao Y P, Wang X P, Dong G H. Numerical simulation and experimental validation of hydrodynamic characteristics of submerged artificial reef in waves [J]. The ocean engineering, 2015, 33(6): 52-61.

# **Appendix**

## **Appendix A: PIV method**

PIV is a non-intrusive, indirect whole field velocity measurement technique, which is an effective way to capture the whole velocity fields instantaneously and to achieve flow visualization by transfer the flow movement to the movement of tracer particles.

### **Principle of Particle Image Velocimetry (PIV)**

The investment of flows was made by hydraulic model carefully planned to extract information about the flow utilizing visualization rather than observe the natural environment directly. PIV as a flow visualization technique has been developed for several decades and widely employed in laboratory studies for different purposes.

The experimental setup of a PIV system typically consists of several subsystem. Normally, tracer particles must be added to the flow. these particles must be illuminated in a plane of the flow within a short time. The displacement of the particle images between the light pulses must be determined through evaluation of the PIV recordings. To be able to handle the great amount of data which can be employing the PIV technique, sophisticated post-processing is required.

Figure 3.1 briefly sketches a typical set-up (Raffle M, Willert C E, Scarano F, et al,2007), although it has some difference with my own experimental setup, but it is very conducive to help us know the basic PIV system. In this PIV system, small particles are added to the flow, a light sheet within the flow is illuminated by laser. It is assumed that the tracer particles

move with local flow velocity. The light scattered by the tracer particles is recorded via a high-speed camera. After development of the photo-graphical PIV recording is digitized by means of scanner. The output of the digital sensor is transferred to the memory of a computer directly.

For evaluation the digital PIV recording is divided in small subareas called “interrogation areas”. The local displacement vector for the images of the tracer particles of the illumination is determined for each interrogation area by means of statistical methods. It is assumed that all particles within in one interrogation area have moved homogeneously. The projection of the vector of the local flow velocity into the plane of the light sheet is calculating considering the time delay between illumination and magnification at imaging

The process of interrogation is repeated for all interrogation areas of the PIV recording. With modern charge coupled device (CCD) cameras (1000\*1000 sensor elements and more) it is possible to capture more than 100 PIV recording per minute. High-speed recording on complementary metal-oxide semiconductor (CMOS) sensors even allows for acquisition in the kHz-range. The evaluation of one digital PIV recording with several thousand instantaneous velocity vectors is of the order of the second with standard computers. If data is required at even faster rates for online monitoring of the flow, dedicated software algorithms which perform evaluations of reduced precision within fraction of a second are commercially available.

From the above description, a summary can be drawn “PIV is a whole field, nonintrusive, indirect velocity measurement technique that can obtain the velocity information with high accuracy and temporal and spatial resolution” (Feng Dejun,2017).

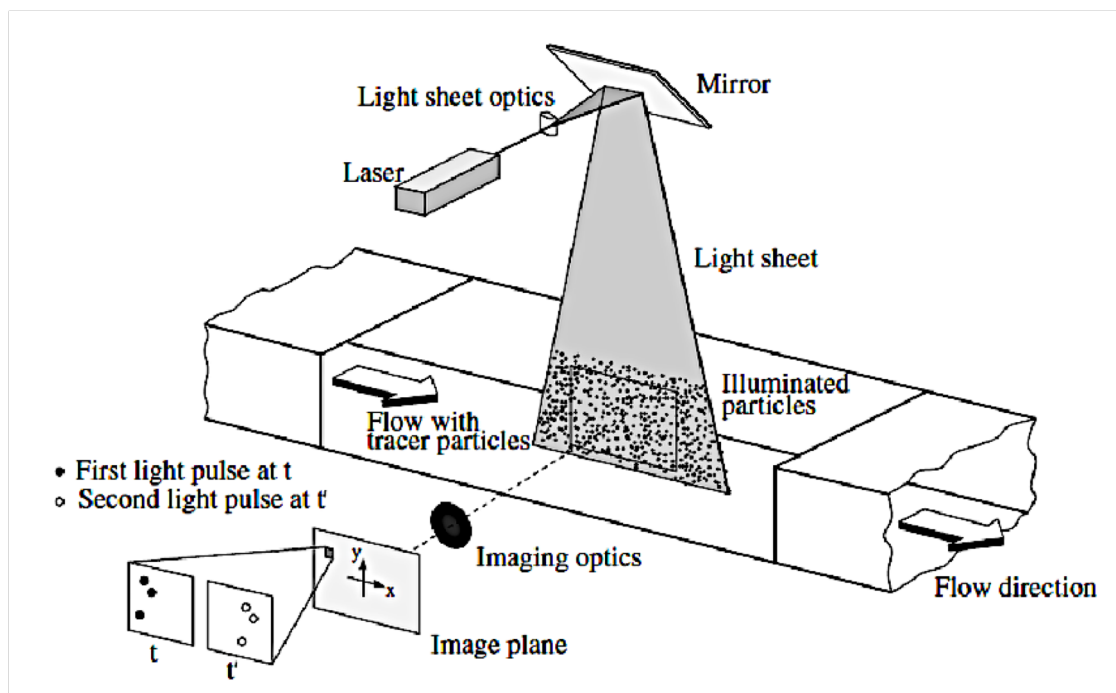


Figure A.1 Sketch of a typical laboratory PIV system (Raffel M, Willert C E, Scarano F, et al)

## Image evaluation method for PIV

From the above chapter, we know that PIV method is an effective way to achieve flow visualization by transferring the flow movement into tracer particles' movement based on certain algorithm. In this part, I will introduce how does the image evaluation method works for PIV by following Raffel 's idea in the book of 'Particle Image Velocimetry), although it has some different with my own experiments.

The main idea of the PIV image evaluation is based on digital spatial correlation analysis. Firstly, we assume we are given a pair of images containing particle images. The particles are illuminated stroboscopically. The second frame is recorded to a short time later during which the particles will have moved according to the underlying flow. Given this pair of images, the most we can hope for is to measure the straight-line displacement of the particle images since the curvature information between the recording instances is lost. Further, the

seeding density is too homogeneous that it is difficult to match up discrete particles. In some cases, the spatial translation of groups of particles can be observed. The image pair can yield a field of linear displacement vectors where each vector is formed by analyzing the movement of localized groups of particles. In practice, this is accomplished by extracting small samples or interrogation windows and analyzing them statically (Figure.3.2).

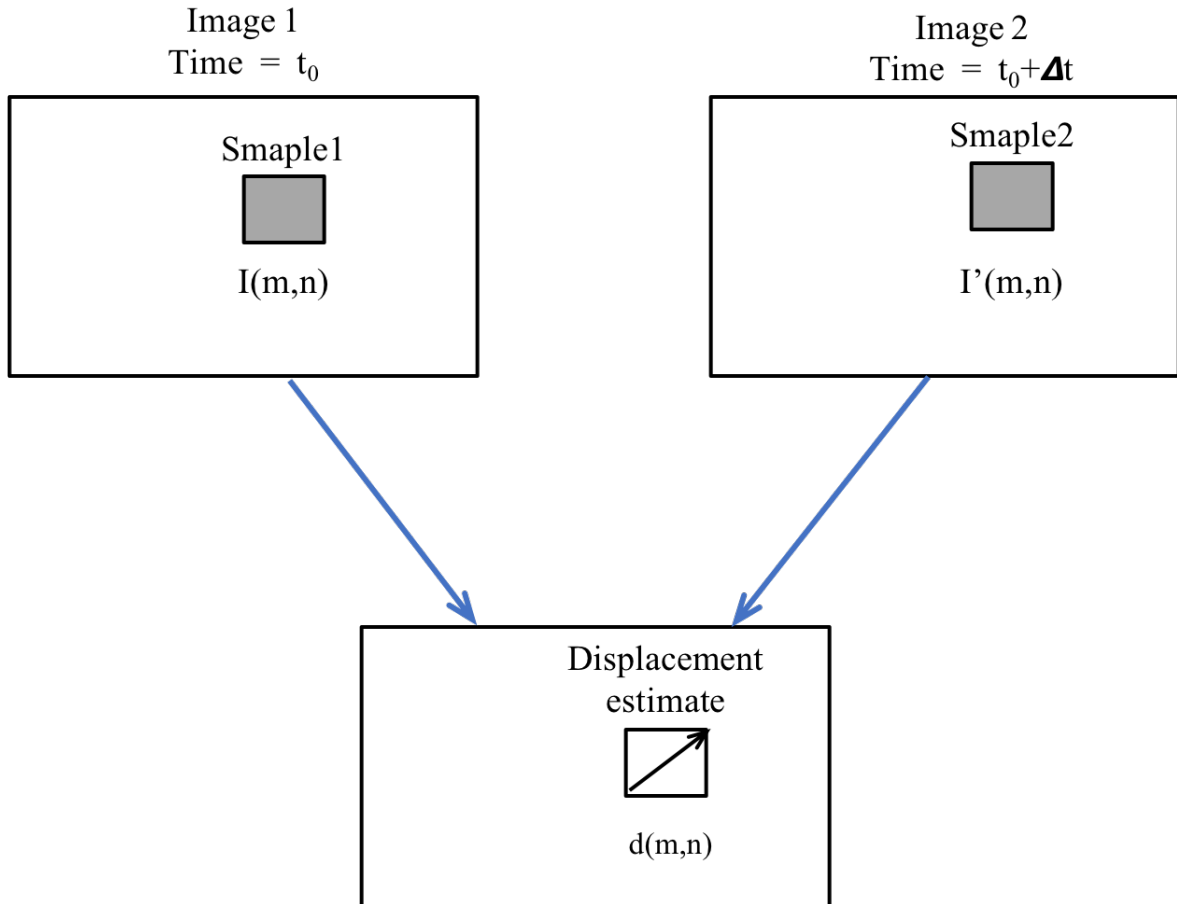


Figure A.2 Sketch for illustration of interrogation window (From Raffel M, 2007)

The method to find the best match between the images in a statistical sense is accomplished by using the discrete cross-correlation function, whose integral function is shown as Eq.A.1:

$$R_{II}(x, y) = \sum_{i=-K}^K \sum_{j=-L}^L I(i, j) I'(i + x, j + y) \quad (A.1)$$

The variable  $I$  and  $I'$  are the samples as extracted from the images where  $I'$  is larger than the template  $I$ . Especially, the template  $I$  is linearly shifted around in the sample  $I'$  without extending over edges of  $I'$ . For each choice of sample shift  $(x,y)$ , the sum of the products of all overlapping pixel intensities produces one cross-correlation value  $R_{II}(x,y)$ . By applying this operation for a range of shifts  $(-M \leq x \leq +M, -N \leq y \leq +N)$ , a correlation planes the size of  $(2M+1) \times (2N+1)$  is formed. This is shown in Figure.A.3. For shift values at which the samples particle images align with each other, the sum of the products of the pixel intensities will be larger than elsewhere, resulting in a high cross-correlation value  $R_{II}$  at this position. Especially, the cross-correlation function statistically measures the degree of match between the two samples for a given shift. The highest value in the correlation plan can then be used as a direct estimate of the particle image displacement.

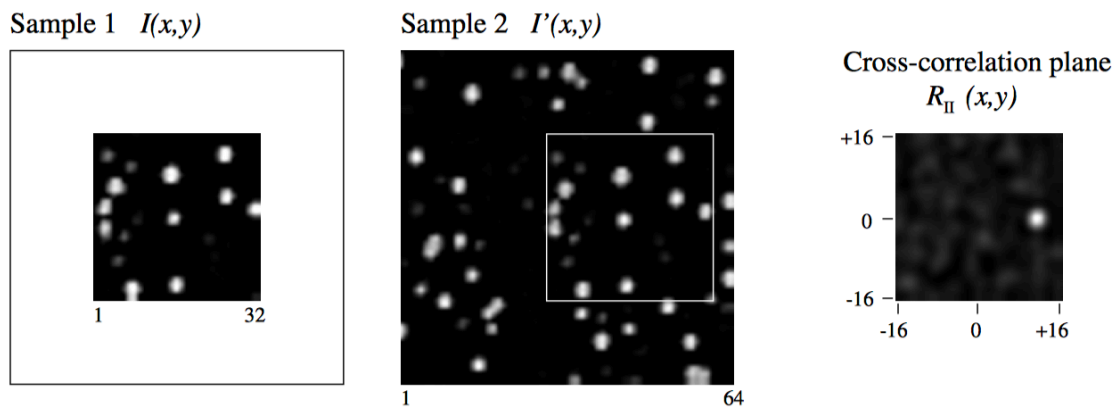


Figure A.3 Sketch of the illustration of the direct cross correlation (From Raffel M, 2007)

Next part I will show the calculation of the correlation coefficient.

For several cases it may be useful to quantify the degree of correlation between the two image samples. The standard cross-correlation function Eq.A.2 will yield different maximum correlation values for the same degree of matching because the function is not normalized. For instance, samples with many (or brighter) particle images will produce much higher correlation values than interrogation windows with fewer (or weaker) particle images. This makes a comparison of the degree of correlation between the individual interrogation windows impossible. The cross-correlation coefficient function normalizes the cross-correlation function Eq.A.2 properly:

$$c_{II}(x, y) = \frac{c_{II}(x, y)}{\sqrt{\sigma_I(x, y)}\sqrt{\sigma'_I(x, y)}} \quad (A.2)$$

where

$$c_{II}(x, y) = \sum_{i=0}^M \sum_{j=0}^N [I(i, j) - \mu_i] [I'(i + x, j + y) - \mu_{I'(x,y)}] \quad (A.3)$$

$$\sigma_I(x, y) = \sum_{i=0}^M \sum_{j=0}^N [I(i, j) - \mu_I]^2 \quad (4.4)$$

$$\sigma'_I(x, y) = \sum_{i=0}^M \sum_{j=0}^N [I'(i, j) - \mu_{I'(x,y)}]^2 \quad (4.5)$$

The value  $\mu_i$  is the average of the template and is computed only once while  $\mu_i(x, y)$  is the average of  $I'$  coincident with the template  $I$  at position  $(x, y)$ . It must be computed for every position  $(x, y)$ .

## Appendix B: program

### Case 1500\_2.a.m

```
clear;clc;

close all

[image_name, image_location]=uigetfile('*.bmp');%to choose the images to be analyzed

image_information=dir(image_location);

image_number=size(image_information,1)-2;

image_first=imread(fullfile(image_location, image_name));

image_height=size(image_first,1);%the size of the image-height

image_width=size(image_first,2);%the size of the image-width

interval_windowcenter=32;

window_height=interval_windowcenter;

window_width=window_height;

horizontal_displacement_max=10;

vertical_displacement_max=10;

yy=image_height-vertical_displacement_max-(window_height-1)/2:-

interval_windowcenter:1+vertical_displacement_max+(window_height-1)/2;

xx=1+horizontal_displacement_max+(window_width-1)/2:interval_windowcenter:image_width-

horizontal_displacement_max-(window_width-1)/2;

% U=nan(13, 15, 399);W=nan(13, 15, 399);

tic
```

```

c1=0;

for ii=1:350 % total pictures minus three ;

    ii

    c1=c1+1;

    image1=imread([image_location, image_information(ii+4).name]);

    aa=image1(:,:,1);

    aa=double(aa);

    aa=intensitycapping_new(aa, 2);

    image2=imread([image_location, image_information(ii+4+1).name]);

    bb=image2(:,:,1);

    bb=double(bb);

    bb=intensitycapping_new(bb, 2);

c2=0;

for kx=xx

    c2=c2+1;

c3=0;

for ky=yy

    c3=c3+1;

    W1=aa(ky-(window_height-1)/2:ky+(window_height-1)/2, kx-(window_width-1)/2:kx+(window_width-1)/2);

    R=nan(2*vertical_displacement_max+1, 2*horizontal_displacement_max+1);

    for mx=kx-horizontal_displacement_max:kx+horizontal_displacement_max

        for my=ky-vertical_displacement_max:ky+vertical_displacement_max

            W2=bb(my-(window_height-1)/2:my+(window_height-1)/2, mx-(window_width-
1)/2:mx+(window_width-1)/2);

```

```

        R(my-ky+vertical_displacement_max+1, mx-
kx+horizontal_displacement_max+1)=corrcoefpiv(W1(:), W2(:));

        end

    end

    [m, ind]=max(R(:));

    [R_y, R_x]=ind2sub(size(R), ind);

    if R_y==2*vertical_displacement_max+1 || R_y ==1 || R_x==2*horizontal_displacement_max+1 || R_x==1

        W(c3, c2, c1)=NaN;

        U(c3, c2, c1)=NaN;

    else

        Py=((R(ind+1)-R(ind-1))/(R(ind+1)-2*R(ind)+R(ind-1)))*1/2;

        Px=((R(ind+2*vertical_displacement_max+1)-R(ind-2*vertical_displacement_max-
1))/(R(ind+2*vertical_displacement_max+1)-2*R(ind)+R(ind-2*vertical_displacement_max-1)))*1/2;

        W(c3, c2, c1)=(R_y-vertical_displacement_max-1-Py);

        U(c3, c2, c1)=(R_x-horizontal_displacement_max-1-Px);

    end

end

end

end

end

toc % after you finished don't forget to save file named UXxyy.mat

```

## Outputimage.m

```
clear;clc

load('UWxyy.mat');

M=2.34/579/(1/500);

u=U;

w=u;

for ii=1:size(U,3)% surfe online of the meaning of size function

    u(:, :, ii)=smoothn(M*U(:, :, ii));

    w(:, :, ii)=smoothn(M*W(:, :, ii));

end

clc

u(:, 23:39, :)=0;

w(:, 23:39, :)=0;

u(6, 3:14, :)=0;

w(6, 3:14, :)=0;

u(7, 4:14, :)=0;

w(7, 4:14, :)=0;

u(8, 7:14, :)=0;

w(8, 7:14, :)=0;

u(9, 8:13, :)=0;

w(9, 8:13, :)=0;

u(10, 9:13, :)=0;

w(10, 9:13, :)=0;

u(11, 11:12, :)=0;

w(11, 11:12, :)=0;

u(15, 15:19, :)=0;

w(15, 15:19, :)=0;

u(14, 17:19, :)=0;
```

```

w(14,17:19,:)=0;

u(13,19,:)=0;

w(13,19,:)=0;

u(18:31, :, :)=0;

w(18:31, :, :)=0;

u(1:5, :, :)=0;

w(1:5, :, :)=0;

[image_name, image_location]=uigetfile('*.*.bmp');% choose the original images
image_information=dir(image_location);

close all

for ii=1:size(U,3)

    f=figure('visible','off');

    imagel=imread([image_location, image_information(ii+4).name]);

    imshow(imagel)

    axis off

    [XX, YY]=meshgrid(xx, flipud(yy));

    hold on

    quiver(XX, YY, 5.*u(:, :, ii), 5.*w(:, :, ii), 'autoscale', 'off', 'LineWidth', 1, 'Color', 'g')

    title(['frame', num2str(ii)])

    set(gca, 'FontWeight', 'bold', 'FontSize', 10)

    xlabel('X [pixel]');

    ylabel('Y [pixel]');

    hold on

    quiver(300, 920, -10*5, 0, 'MaxHeadSize', 1, 'autoscale', 'off', 'Linewidth', 1, 'Color', 'g')

    text(100, 920, '\color{green} 10 cm/s', 'Fontweight', 'bold', 'FontSize', 15)

    box off

    saveas(gcf, ['E:\navyzhu\matlab_data\result_1\' , 'frame--' , num2str(ii), '.bmp']);

end

```